ARTICLE

Philippine marine natural product scaffolds as inhibitors of DNA damage response pathways with promising binding propensity, stability, and pharmacokinetic profiles

Juliana Laine G. Rublico[1], Francesca Danielle S. Baysa[1], Jamielle C. Sarga[1], Casandra Marie B. Sibug[1], Edward Brian M. Ranjo[1], Mark Tristan J. Quimque[3], Jay Carl M. Agbay[4], Joe Anthony H. Manzano[1,2], and Carl Jay Laurenciano*[1]

[1]Department of Biological Sciences, College of Science, University of Santo Tomas, 1008 Manila, Philippines
[2]UST Laboratories for Vaccine Science, Molecular Biology, and Biotechnology, Research Center for Natural and Applied Sciences, University of Santo Tomas, 1008 Manila, Philippines
[3]Chemistry Department, College of Science and Mathematics, Mindanao State University – Iligan Institute of Technology, Tibanga 9200, Iligan City, Philippines
[4]Department of Science and Technology - Philippine Science High School – Central Mindanao Campus, 9217 Balo-i, Lanao del Norte, Philippines

Since identifying effective compounds is time-consuming and costly, computational drug-discovery methods now enable high-throughput screening of bioactive molecules. Philippine marine natural products (MNPs) were computationally screened against four targets in the DNA damage response (DDR) pathways: Poly (ADP-ribose) polymerase 1 (PARP-1), Histone Deacetylase 2 (HDAC2), and topoisomerases I and II (TOPOI and TOPOII). These targets are crucial in various diseases, including cancer. A total of 27 MNPs were screened through molecular docking. Most favorable complexes were further analyzed for pharmacokinetic and drug-likeness profiling, visualization and molecular interaction analysis, and molecular dynamics (MD) simulations. Several MNPs demonstrated strong binding affinities to DDR targets, along with promising pharmacokinetic profiles supporting their drug candidacy including Ningalin B for PARP-1; Perophoramidine for HDAC2; Ulithiacyclamide B for TOPOI; and Patellamide C for TOPOII. MD simulations affirmed the stability of the best complexes via root-mean-square deviation and fluctuation, radius of gyration, and interaction energy analyses. Overall, the *in silico* results highlight the potential of Philippine MNPs—especially Ningalin B, Perophoramidine, Ulithiacyclamide B, and Patellamide C—as natural-product inhibitors of DDR pathways relevant to anticancer drug discovery.

*Corresponding author
Email Address: cdlaurenciano@ust.edu.ph
Date received: 08 August 2025
Dates revised: 01 October 2025, 31 October 2025, 18 December 2025,
Date accepted: 25 December 2025
DOI: https://doi.org/10.54645/202518SupEOX-42

KEYWORDS

DNA damage response; marine natural products; molecular docking; molecular dynamics

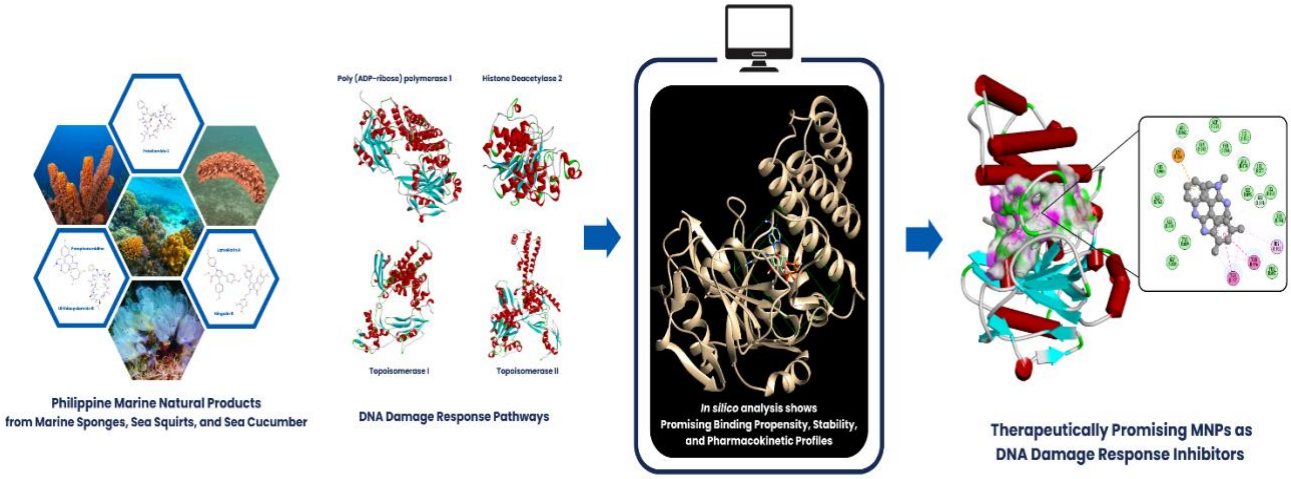

***In silico* activities of various Philippine Marine Natural Products as potential DNA Damage Response inhibitors**

INTRODUCTION

The maintenance of genomic integrity through efficient repair of deoxyribonucleic acid (DNA) damage is fundamental to cellular survival and function. DNA damage response (DDR) pathways are essential in recognizing and rectifying various DNA lesions, including single-strand breaks (SSBs), double-strand breaks (DSBs), and crosslinks, primarily via base excision repair (BER), nucleotide excision repair (NER), and homologous recombination (Chatterjee and Walker 2017). In oncology, DDR mechanisms are of particular interest as cancer cells frequently exploit these pathways to overcome genotoxic stress and maintain proliferation. Consequently, recent advances have highlighted DNA damage response modulation (DDRM) inhibitors as effective adjuvant therapies, enhancing the cytotoxicity of chemotherapy and radiotherapy by selectively impairing the DNA repair capabilities of cancer cells (Cheng et al. 2022).

Key enzymes involved in DDRM include Poly (ADP-ribose) polymerase 1 (PARP-1), histone deacetylase 2 (HDAC2), and topoisomerases I and II (TOPOI and TOPOII), all of which play critical roles in preserving genome stability and cell cycle progression. PARP-1 binds competitively to DNA damage sites and catalyzes poly (ADP-ribose) synthesis to recruit DNA repair proteins to single-stranded breaks; its inhibition results in persistent DNA strand breaks that ultimately lead to cancer cell death (Peng et al. 2022). HDAC2 modulates gene expression by deacetylating histones, resulting in chromatin compaction and transcriptional repression (Seto and Yoshida 2014). Accordingly, HDAC inhibitors prevent histone deacetylation, thereby hindering chromatin condensation required for mitosis and exhibiting anticancer potential (Li and Sun 2019). Topoisomerases resolve DNA supercoiling during replication and repair, and their inhibition prevents DNA ends from re-ligating, inducing cytotoxic lesions (Pommier 2009). TOPOI primarily addresses SSBs, whereas TOPOII resolves DSBs (Baker et al. 2008; McClendon and Osheroff 2007). Emerging evidence further indicates that marine natural products (MNPs) possess bioactive compounds capable of modulating DDR pathways, positioning them as promising candidates for anticancer drug discovery.

The Philippines, an archipelagic nation located at the heart of the Coral Triangle, represents a valuable reservoir of marine natural products with immense pharmaceutical potential. Its archipelagic setting of over 7,600 islands and extensive coral reef systems provides unique ecological niches that foster the evolution of structurally diverse and biologically potent marine secondary metabolites (Al-Asif et al. 2022). Marine organisms from Philippine waters, particularly sponges, sea squirts, and sea cucumbers, are known to produce metabolites with pharmacological properties distinct from those found in temperate environments (Concepcion et al. 2014). This biodiversity constitutes a largely untapped chemical reservoir that could yield novel scaffolds for drug discovery with promising DDR-modulating activity, although their mechanisms and therapeutic potential remain less explored compared to synthetic DDRM inhibitors. The significance of marine-derived compounds in pharmacology is exemplified by the approval of PRIALT® (Ziconotide) in 2004, a conotoxin derived from *Conus magnus* venom and now used clinically for chronic pain management due to its potent and selective action on ion channels and membrane receptors (Molinski 2009; Gomez et al. 2019). More recently, Filipino marine bioprospecting initiatives have explored marine sponges for the development of combination therapies against cancer, further underscoring the untapped potential of local MNPs in oncological therapeutics (Acyatan et al. 2024).

In this study, the selected compounds are referred to as "Philippine MNPs" as they originate from marine species documented in Philippine waters, with their initial extraction and characterization reported in prior studies conducted elsewhere (Karim et al. 2018; Sajwani 2019). As demonstrated by Concepcion et al. (2014), bioactive compounds from Philippine ascidians and sponges have been successfully isolated and elucidated using advanced spectroscopic techniques. A total of 27 compounds were selected based on the following criteria: (1) reported bioactivity associated with DNA damage response modulation, such as Didemnin B from *Tridemnum solidum* (Lee et al. 2012), Perophoramidine from *Perophora namei* (Palanisamy et al. 2017), and Patellamides and Ascidiacyclamide from *Lissoclinum patella* (Schmidt et al. 2005); (2) availability of high-quality three-dimensional structures and reliable chemical data in PubChem; (3) structural diversity representing distinct chemical scaffolds from Philippine marine species; and (4) origin from marine organisms recognized as native inhabitants of Philippine marine ecosystems based on biodiversity records and ecological surveys (Longakit et al. 2005; Shenkar and Swalla 2011).

Despite growing interest, the role of MNPs in targeting DDR pathways remains underexplored. Challenges persist in the isolation, characterization and *in vitro* and *in vivo* evaluation of marine-derived compounds due to the complexity and resource-intensive nature of experiments and analysis. To address these limitations, computational approaches have become increasingly valuable tools in anticancer drug discovery. In fact, previous studies have demonstrated the utility of computational

modeling in identifying novel compounds targeting cancer-related proteins (Malaluan et al. 2022; Manzano et al. 2022; Ibana et al. 2024; Manzano et al. 2024a; Manzano et al. 2025). Nevertheless, comprehensive computational screening of Philippine-derived marine compounds remains limited. This gap highlights the need for systematic *in silico* screening to uncover novel anticancer candidates from Philippine marine ecosystems.

This study therefore integrates molecular docking, molecular dynamics simulations, and pharmacokinetic predictions to identify promising Philippine MNPs as potential DDR inhibitors for anticancer therapy development.

MATERIALS AND METHODS

MNP and DDRM collection

The DDRM PARP-1, HDAC2, TOPOI, and TOPOII were selected as target receptors. Their 3D structures were retrieved from the RCSB Protein Data Bank (https://www.rcsb.org) using the following Protein Data Bank (PDB) IDs: 4UND (PARP-1), 3MAX (HDAC2), 1T8I (TOPOI), and 4FM9 (TOPOII). Clinically approved inhibitors were used as positive controls: olaparib and talazoparib for PARP-1; vorinostat and panobinostat for HDAC2; topotecan and camptothecin for TOPOI; and etoposide and doxorubicin for TOPOII.

A total of 27 Philippine marine natural products (MNPs), derived from sea squirts, marine sponges, and sea cucumbers, were selected as ligands for the docking studies (Table 1). Canonical Simplified Molecular Input Line Entry System (SMILES) notations for each MNP were obtained from PubChem (https://pubchem.ncbi.nlm.nih.gov). Figure 1 depicts the 2D structures of the 27 MNPs, generated with MolDraw (https://moldraw.com/). These SMILES strings were converted into SYBYL mol2 format using UCSF Chimera 1.17.3 (Huang et al. 2018) for subsequent docking studies (Manzano et al. 2024; Tan et al. 2024).

Table 1: List of All Marine Natural Products, their Species of Origin, and Existing Research on their Mechanism of Action.

MNP	Species	Location	Mechanism of Action	Classification
Sea Squirts				
Didemnin B	*Tridemnum sp.*	Apo Reef, Mindoro Island	Inhibition of protein synthesis by acting on Eukaryotic translation elongation factor 1 alpha 1 (EEF1A1) (Hetherington et al. 2016).	Cyclic peptide
Diplosoma Ylidene-2	*Diplosoma virens*	Apo Reef, Mindoro Island Cebu	Caspase activation via the mitochondrial/cytochrome C stress pathway (Ogi et al. 2008).	Alkaloid
Perophoramidine	*Perophora namei*	Zamboanga Peninsula	PARP cleavage (Ishida & Takemoto 2013).	Cyclic peptide
Patellamides	*Lissoclinum patella*	Mindoro Island	Exact mechanism is not known to date (Ramadhani et al., 2022).	Cyclic peptide
Ascidiacyclamide	*Lissoclinum patella*	Mindoro Island	DNA damage, but exact mechanism is not known to date (Chen et al. 2018).	Cyclic peptide
Cycloxazoline	*Lissoclinum bistratum*	Mindoro Island	Delays cells in S-phase from entering the G2/M phase (Zhang et al., 2021).	Cyclic peptide
Sansalvamide A	*Lissoclinum sp.*	Mindoro Island	Inhibition of topoisomerase I and G(1) cell cycle arrest (Zheng et al. 2011).	Cyclic peptide
Ulithiacyclamide B	*Lissoclinum patella*	Mindoro Island	Decreases cell viability, but exact mechanism is yet to be identified (Ahmed et al. 2022).	Cyclic peptide
Marine Sponge				
Ilimaquinone	*Dactylospongia*	San Francisco, Cebu	Inhibition of PDK1 activity	Quinone /

	elegans		(Kwak et al. 2020).	Terpenoid
Ningalin B	*Iotrochota sp.*	San Francisco, Cebu	P-glycoprotein inhibition (Dantzic et al. 2018).	Alkaloid
Lamellarins	*Iotrochota sp.*	San Francisco, Cebu	Topoisomerase I inhibition leading to the activation of a nuclear pathway; targets mitochondria to directly induce apoptosis (Bailly 2015).	Alkaloid
Microcionamide A	*Clathria (Thalysias) abietina*	Philippines	PARP cleavage and caspase-3 activation (Mokhlesi et al. 2017).	Cyclic peptide
Pseudoceratinine A	*Pseudoceratina verrucosa*	Marigondon, Cebu	Not known	Alkaloid
Spheciosterol sulfates	*Spheciospongia sp*	San Francisco, Cebu Mindoro La Union Ilocos Norte Ilocos Sur	Inhibits NF-κB activation and PKC-zeta (Whitson et al. 2008).	Sulfated sterol
Topsentiasterol sulfate E	*Spheciospongia sp*	San Francisco, Cebu Mindoro La Union Ilocos Norte Ilocos Sur	Inhibits NF-κB activation and PKC-zeta (Whitson et al. 2008).	Sulfated sterol
Sea Cucumber				
Frondoside A	*Cucumaria frondosa*	Philippines	Inhibition of p21-activated kinase 1 (PAK1); caspase 3 activation; PARP cleavage (Adrian & Collin 2018).	Triterpenoid / sulfated saponin

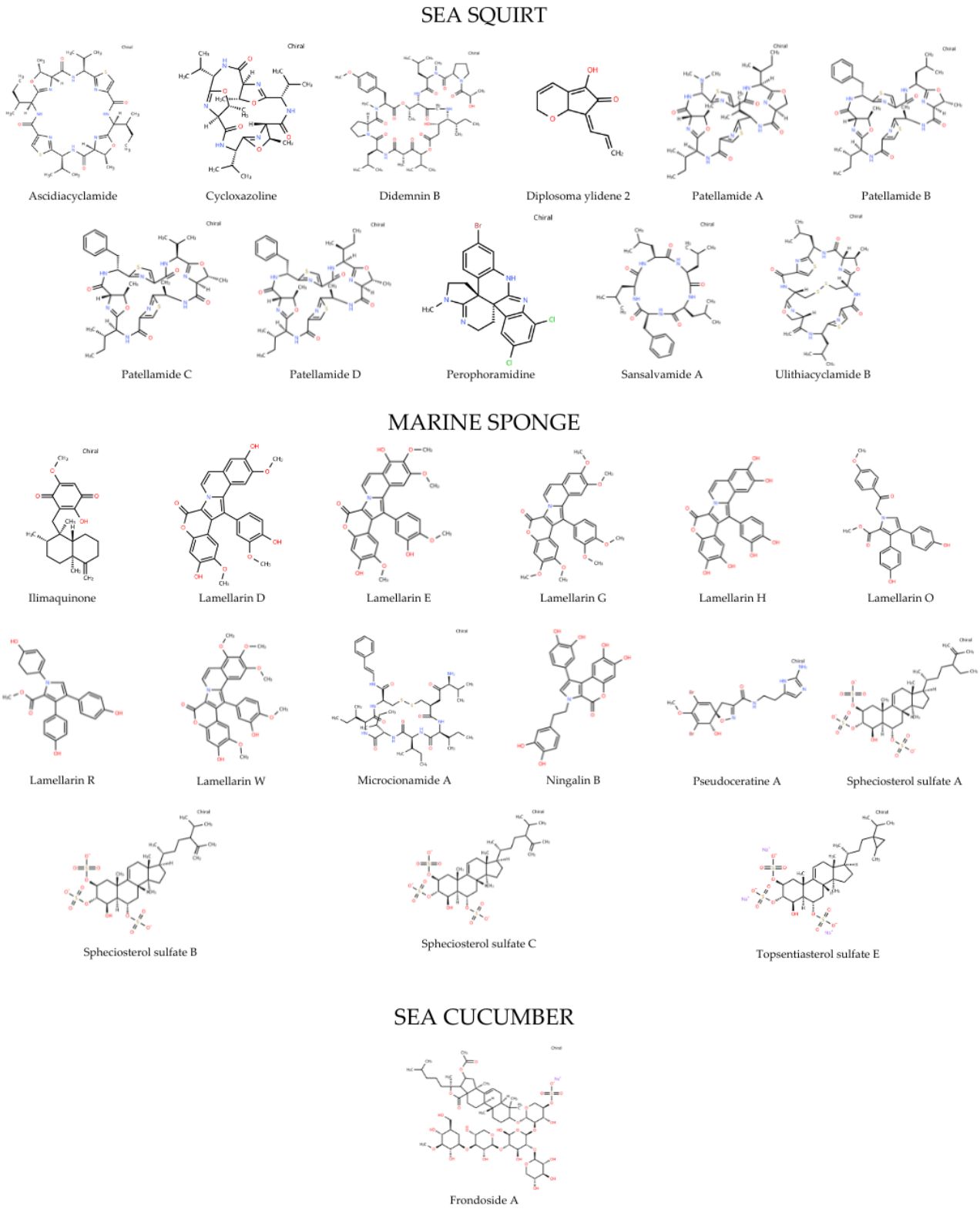

Figure 1: 27 Structures of Marine Natural Products (MNPs) from Sea Squirts, Marine Sponges, and Sea Cucumber drawn in MolDraw.

Ligand and Receptor Preparation

The 27 MNP ligands were geometrically optimized using Avogadro version 1.2.0 (Hanwell et al. 2012). For the receptor proteins, refinement was performed in UCSF Chimera, including isolation of specific protein chains based on active site localization. Selected chains were specified in their respective RCSB PDB depositions, confirming their biological relevance for docking. Chain B was selected for PARP-1 (Thorsell et al. 2017) as it contains the catalytic domain co-crystallized with talazoparib. Meanwhile, the active site for HDAC2 to an N-(2-aminophenyl)benzamide inhibitor was seen in Chain as indicated in the PDB entry (Bressi et al. 2010). For TOPOI, Chain A represents the catalytic domain complexed with camptothecin and a DNA duplex, with PDB annotation confirming its role as physiologically relevant cleavage complex (Staker et al. 2005). Chain A was also chosen for TOPOII as it corresponds to the DNA-bound catalytic core, and its PDB deposition specifies this as targeted by inhibitors such as

etoposide (Wendorff et al. 2012). Non-standard residues and water molecules were removed to expose and simplify the binding pockets. Receptor energy minimization was performed, and Gasteiger charge distribution was applied (Fernandez et al. 2021).

Molecular Docking and Visualization

Molecular docking was conducted using UCSF Chimera 1.17.13 (Huang et al., 2018). Structures for receptors: PARP-1, HDAC2, and TOPOI were already co-crystallized with their respective inhibitors. The TOPOII structure was co-crystallized with DNA rather than an inhibitor. Although not in the apo form, this DNA-bound structure still represents the enzyme's catalytic conformation suitable for inhibitor docking. Grid box parameters were set to cover the active binding site of each receptor. Dimensions of the grid box were manually adjusted to ensure coverage of the active binding site, while excluding irrelevant regions. The specific grid center and size values used for each receptor are summarized in Table 2. AutoDockTools 1.5.7 was used for docking configuration, and the AutoDock Vina-based scoring function was applied to estimate ligand-receptor BE (kcal/mol), which estimates the free energy of binding by combining weighted terms for van der Waals forces, hydrogen bonds, electrostatic hydrophobic bonds, and torsional entropy (Eberhardt et al. 2021). All MNPs and positive controls were docked against each receptor, and the ten MNPs with the lowest BE values were selected for visualization of molecular interactions and drug-likeness evaluation. Binding site interactions were visualized using BIOVIA Discovery Studio 2021. The docking protocol was validated by calculating the root mean square deviation (RMSD) between the co-crystallized and re-docked ligands as presented in Supplementary Table 1. The RMSD values for all target proteins were less than 2 Å, indicating that the docking procedure reliably reproduced the experimentally observed ligand–protein conformations (Magpantay et al. 2021; Manzano et al. 2024b).

Table 2: Grid Box Center Coordinates, Dimensions, and Binding Site References for Target Receptors: PARP-1, HDAC2, TOPOI, and TOPOII

Receptors	Grid Center (X,Y,Z)	Grid Size (X,Y,Z)	Binding Site References
PARP-1	30.7679, 50.0061, 217.503	19.212, 12.6439, 34.4957	Co-crystallized inhibitor (Thorsell et al. 2017)
HDAC2	72.8783, 26.5585, -9.15621	23.5245, 33.6619, 33.6562	Co-crystallized inhibitor (Bressie et al. 2010)
TOPOI	21.2864, -6.13234, 25.4773	57.5465, 33.9398, 40.3403	Co-crystallized inhibitor (Staker et al. 2005)
TOPOII	29.2045, 47.4878, 19.8507	29.583, 49.4614, 40.1555	DNA-binding Catalytic Site (Wendorff et al. 2012)

Drug-likeness Predictions

The MNP ligands were evaluated for pharmacokinetic properties and drug-likeness using the SwissADME web tool (Daina et al., 2017). Lipinski's Rule of Five (LRo5) criteria were used to assess drug-likeness, including: molecular weight < 500 Da, lipophilicity (MLogP) < 5, number of hydrogen bond acceptors (NH or OH) < 10, and hydrogen bond donors (NH or O) < 5, whereas gastrointestinal tract absorption and Blood Brain Barrier (BBB) permeability were utilized to assess favorable pharmacokinetic properties (Quimque et al. 2021; Karami et al. 2022). Accordingly, this evaluation represents basic *in silico* absorption descriptions and preliminary screening rather than a comprehensive pharmacokinetic analysis.

Molecular Dynamics

Selected ligand-receptor complexes were subjected to molecular dynamics (MD) simulations based on two criteria: (1) the lowest BE and (2) favorable drug-likeness properties. This multi-faceted approach of choosing candidates for MD simulations values favorable docking scores as the most impactful factor, but MNPs with more than one Lipinski criteria violation and unfavorable pharmacokinetic permeability and absorption, prompting less favorable drug-like properties than majority of the positive controls, have been excluded. Simulations were performed using GROMACS 2022.1 under Ubuntu Linux 22.04 (Abraham et al., 2025). Protein topologies were generated using the CHARMM36 force field with a TIP3P water model, while ligand topologies were created using the CHARMM General Force Field (CGenFF). Each system was solvated in a dodecahedral box using the *spc216.gro* coordinate file, which is treated as TIP3P under the CHARMM36 topology, and neutralized with Na^+ and Cl^- ions.

Energy minimization was performed using the steepest descent integrator for 5000 steps. The Particle Mesh Ewald (PME) method was used to account for Coulomb and van der Waals interactions. After equilibration, production runs were carried out for 50 ns at 300 K (26.85 °C). System trajectories were recorded every 10 ps and subsequently analyzed to determine root mean square deviation (RMSD) and root mean square fluctuation (RMSF). Interaction energies (IE) were calculated using the g_energy tool from GROMACS, based on the 50-ns simulation data. The interaction energy of each complex was calculated as the sum of short-range Coulomb and Lennard-Jones interactions:

$$IE = E_{Coul-SR} + E_{LJ-SR}$$

RESULTS AND DISCUSSION

Binding Affinity Analysis

Molecular docking revealed notable binding affinities of various MNPs to key DDRM PARP-1, HDAC2, TOPOI, and TOPOII. Each of the four enzymes plays a distinct and therapeutically relevant role in cancer biology. PARP-1 is a critical target, particularly in BRCA1/BRCA2-deficient tumors that rely on PARP-mediated repair of DNA single-strand breaks. Inhibiting PARP-1 in such contexts leads to synthetic lethality, selectively killing cancer cells (Hopkins et al. 2019). HDAC2, implicated in chromatin remodeling and transcriptional repression, is a validated target for both cancer and neurodegenerative diseases due to its influence on cell cycle progression and apoptosis (Jo et al. 2023). TOPOI is vital for relieving torsional strain during DNA replication and transcription. Its transient cleavage complex is a pharmacological vulnerability exploited by selective inhibitors, offering a tailored strategy for tumors with defective DNA repair checkpoints (Pommier 2006). TOPOII, essential for chromosomal segregation during mitosis, is targeted by inhibitors that trap the DNA-enzyme complex, inducing DNA damage and apoptosis in proliferating cells. Remarkably, several MNPs exhibited more favorable binding energy (BE) to these target proteins than clinically established drugs, highlighting their potential as lead compounds for targeted anticancer therapy.

Table 3 presents the calculated binding energies (BE) and interacting residues for the 27 MNPs against the four receptors.

Among the MNPs, Ningalin B showed the strongest binding to PARP-1 (–11.5 kcal/mol), Perophoramidine exhibited the highest affinity for HDAC2 (–8.1 kcal/mol), Didemnin B demonstrated the most favorable interaction with TOPOI (–9.8 kcal/mol), and Patellamide C displayed the strongest binding to TOPOII (–10.7 kcal/mol). These negative BE values indicate spontaneous and energetically favorable ligand–receptor interactions. Notably, several MNPs demonstrated comparable or higher binding affinities relative to positive control drugs, suggesting their potential utility as alternative or complementary therapeutic agents. Overall, the observed binding trends indicate that selected Philippine MNPs can match or exceed reference compounds, with binding likely mediated by a combination of favorable structural and chemical features (Vivek-Ananth et al. 2020).

Table 3: BE of positive controls and MNPs against the four DDRMs

Ligands	Binding energy score (kcal/mol)			
	PARP1	HDAC2	TOPOI	TOPOII
Positive Controls				
Olaparib	-11.1	—	—	—
Talazoparib	-10.1	—	—	—
Vorinostat	—	-7.0	—	—
Panobinostat	—	-7.1	—	—
Topotecan	—	—	-8.9	—
Camptothecin	—	—	-8.9	—
Etoposide	—	—	—	-9.8
Doxorubicin	—	—	—	-9.4
Sea Squirt				
Ascidiacyclamide	4.8	-6.3	-8	-7.8
Cycloxazoline	-5.8	-6.7	-8	-8
Didemnin B	31.6	-7.3	-9.8	-10
Diplosoma Ylidene-2	-6.8	-6.3	-6.1	-6.5
Patellamide A	33.9	-7.3	-8.7	-10.3
Patellamide B	20	-7.3	-9.1	-9.5
Patellamide C	34.4	-7.6	-8.9	-10.7
Patellamide D	-0.2	-8	-8.5	-8.7
Perophoramidine	-10.8	-8.1	-7.9	-8.8
Sansalvamide A	-9.4	-7.1	-7.7	-7.8
Ulithiacyclamide B	15.9	-7.6	-9.5	-9.2
Marine Sponge				
Ilimaquinone	-8.9	-6.3	-7.2	-8.3
Lamellarin D	-5.7	-6.5	-8.4	-8.2
Lamellarin E	-7.3	-6.7	-7.5	-8.7
Lamellarin G	-6.7	-6.2	-7.8	-8.2
Lamellarin H	-9.7	-7.4	-8.9	-8.8
Lamellarin O	-9.9	-7.1	-7.8	-9
Lamellarin R	-10	-7.6	-8.1	-9
Lamellarin W	-5.2	-6.7	-8	-8.2
Microcionamide A	-2.2	-5.4	-7.6	-8.1
Ningalin B	-11.5	-7.7	-8.9	-10.1
Pseudocreatine A	-8.7	-6.6	-7.4	-7.3

Spheciosterol sulfate A	-1.4	-1.3	-1.2	-1.3
Spheciosterol sulfate B	-1.4	-1.3	-1.2	-1.3
Spheciosterol sulfate C	-1.4	-1.3	-1.2	-1.3
Topsentiasterol sulfate E	-1.4	-1.3	-1.2	-1.3
Sea Cucumber				
Frondoside A	23.3	-8	-8.2	-10.3

Drug-likeness and Pharmacokinetic Profile Analysis

SwissADME analysis was performed on the 18 MNPs with the most favorable docking energies (10 per receptor, with overlaps). These were evaluated for drug-likeness and pharmacokinetic properties. SwissADME was employed to evaluate the druggability of the MNPs based on their pharmacokinetic parameters, Lipinski's Rule of Five, absorption and permeability, and Pan Assay Interference Structures (PAINS) alert. Lipinski's Rule of Five serves as a foundational guideline in rational drug design by predicting oral bioavailability based on molecular properties (Bitew et al. 2021). This assessment is critical for identifying potential lead compounds with favorable pharmacokinetic profiles. PAINS alerts identify motifs such as catechols and quinones that may cause non-specific binding in screening assays (Daina et al. 2017).

Among the 18 MNPs, only Lamellarin R fully satisfied all criteria, exhibiting no violations, high gastrointestinal (GI) absorption, and no PAINS alert. This profile mirrored those of positive controls Olaparib and Talazoparib. Other MNPs namely Perophoramidine, Ilumaquinone, Lamellarin O, and Pseudoceratine A have demonstrated favorable pharmacokinetic profiles with only minor violations and high GI absorption, indicating strong potential for further optimization. Moreover, the general Lipinski cutoff is MLogP<5; however, some MNPs reported drug-likeness violations when MLogP exceeds 4.15. For example, Perophoramidine had MLogP 5.51, slightly above the Lipinski cutoff, resulting in a rule violation. This highlights that computational cutoffs can vary and may require context-specific interpretation. Perophoramidine likewise emerged as a compelling multitarget inhibitor. Guha et al. (2022) synthesized a pentacyclic core derivative of Perophoramidine via blue LED mediated cyclopropanation, which exhibited cytotoxic activity across various cancer cell lines and induced DNA damage characteristic of PARP inhibition. The docking results supported its strong affinity for PARP-1, affirming its role as a potential modulator of DDR signaling. In contrast, cyclic peptides like Patellamides, Ulithicyclamide B, Dedemnin B, and Frondoside A have accumulated multiple Lipinski violations due to their molecular weight, which has resulted in poor GI absorption and limited permeability. Despite Lipinski violations, we still consider these MNPs for further study because of their highly favorable binding energies. Future work could involve optimizing their structures to improve drug-likeness. Synthetic modifications, such as those employed by Yerien et al. (2016) may be utilized to address this issue of drug-likeness. One of the common issues among these non-drug-like MNPs was high molecular weight, which can hinder distribution within biological systems (Coimbra et al. 2021). Additionally, a high number of hydrogen bond donors, which are NH or OH groups (>5) and acceptors (N or O atoms >10) may reduce membrane permeability, thus negatively impacting oral bioavailability (Kenny 2022). Despite these challenges, structural optimization strategies may be pursued to enhance druggability. Such strategies may include chemical substitutions or elimination of hydroxy and amine groups, as well as aliphatic fluorination to improve physicochemical properties (Yerien et al. 2016). Furthermore, the application of advanced drug delivery systems could improve the pharmacokinetic behavior of otherwise non-ideal compounds. In addition, technologies such as liposome-based nanoparticles have shown promise in enhancing drug solubility, stability, and targeted delivery (De Leo et al. 2022). These approaches open avenues for repurposing MNPs that initially exhibit suboptimal drug-likeness into viable drug templates.

To address the risk of non-specific binding, the PAINS alerts from SwissADME of each candidate molecule were also taken into consideration. Most MNPs were free of PAINS alert, however, Ningalin B, Lamellarin H, and Ilimaquinone all presented one PAINS alert each, meaning specific motifs in their structures (catechol for Ningalin B and Lamellarin, quinone for Ilimaquinone), may contribute to the non-specific binding of these molecules (Magalhães et al., 2021). This may serve as an allusion to the molecules' ability to target multiple DDRMs, which can also be observed in the docking scores of these complexes, performing well across all receptors. Notably, Ningalin B has been previously reported for its P-glycoprotein (P-gp) inhibitory activity in breast cancer cell lines overexpressing P gp. Among nine synthesized permethyl analogs, permethyl Ningalin B derivative demonstrated strong modulation of P gp activity (Wang et al. 2015). Molecular docking further suggested Ningalin B's capacity to interact with multiple DDR related targets, broadening its potential use in oncology. Functional group analysis indicated that catechol and dimethoxy substitutions were critical for P-gp inhibition, and these same electron donor groups have contributed to receptor binding in the docking results, highlighting overlapping features that may underlie multitarget activity of this compound (Kathawala et al. 2015). Despite PAIN alerts, structural modification of these compounds can transform natural scaffolds into potent modulators with improved druggability (Newman and Cragg 2020).

Overall, the analysis of these 18 MNPs demonstrates although these compounds may deviate from conventional drug-like properties, some have shown promising pharmacokinetic profiles comparable to approved commercially available drugs. Meanwhile, other compounds like Patellamides and Frondoside A may require synthetic optimization to overcome their limitations and violations. The findings suggest the balance between structural novelty and drug-likeness, showing the potential of MNPs as promising modulators of DDR pathways. This assessment was restricted to rule-based drug likeness absorption predictions. While useful for early-stage filtering, these parameters do not capture metabolic stability and physiological effects. Therefore, the reported results should be interpreted as preliminary indicators of oral drug-likeness.

Table 4: Drug-likeness and pharmacokinetic profile of top MNPs according to Lipinski's rule of five.

Compound	Molecular weight (<500 g/mol)	H-bond donors (<5)	H-bond acceptors (<10)	Lipophilicity (MLogP<5)	Lipinski Violations	Drug-likeness	PAINS	Pharmacokinetic absorption/ permeability	
								GI absorption	Blood brain barrier
Positive controls									
Olaparib *PARP-1*	434.46	1	5	3.09	None	Yes	0 alert	High	No
Talazoparib *PARP-1*	380.85	2	6	3.16	None	Yes	0 alert	High	No
Panobinostat *HDAC2*	349.43	4	3	2.31	None	Yes	1 alert: indol_3yl_alk	High	Yes
Vorinostat *HDAC2*	264.32	3	3	1.83	None	Yes	0 alert	High	No
Topotecan *TOPOI*	421.45	2	7	0.98	None	Yes	1 alert: mannich_A	High	No
Camptothecin *TOPOI*	348.35	1	5	1.64	None	Yes	0 alert	High	No
Etoposide *TOPOII*	588.56	3	13	-0.14	MW>500 NorO>10	No	0 alert	Low	No
Doxorubicin *TOPOII*	543.52	6	12	-2.10	None	No	1 alert: quinone_a	Low	No
Marine Natural Products									
Didemnin B *Sea squirt*	1112.35	5	15	-1.05	MW>500 NorO>10	Error	0 alert	Low	No
Diplosoma Ylidene-2 *Sea squirt*	190.20	1	3	0.41	None	Yes	0 alert	High	Yes
Patellamide A *Sea squirt*	742.95	4	10	0.35	MW>500 NorO>10	No	0 alert	Low	No
Patellamide B *Sea squirt*	776.97	4	10	0.67	MW>500 NorO>10	No	0 alert	Low	No
Patellamide C *Sea squirt*	762.94	4	10	0.5	MW>500 NorO>10	No	0 alert	Low	No
Patellamide D *Sea squirt*	776.97	4	10	0.67	MW>500 NorO>10	No	0 alert	Low	No
Perophoramidine *Sea squirt*	476.20	1	2	5.51	MLOGP>4.15	Yes	0 alert	High	Yes
Sansalvamide A *Sea squirt*	599.80	5	5	1.46	MW>500	Yes	0 alert	Low	No
Ulithiacyclamide B *Sea squirt*	797	4	10	0.14	MW>500 NorO>10	No	0 alert	Low	No
Ilimaquinone *Marine sponge*	358.47	1	4	2.26	None	Yes	1 alert: quinone_A	High	Yes
Lamellarin D *Marine Sponge*	499.47	3	8	1.87	None	Yes	0 alert	Low	No

Lamellarin E *Marine sponge*	531.51	3	9	1.43	MW>500	Yes	0 alert	Low	No
Lamellarin H *Marine sponge*	459.40	6	8	0.94	NHorOH> 5	Yes	1 alert: cathechol_A	Low	No
Lamellarin O *Marine sponge*	457.47	2	6	2.10	None	Yes	0 alert	High	No
Lamellarin R *Marine sponge*	401.41	3	5	2.63	None	Yes	0 alert	High	No
Ningalin B *Marine sponge*	461.42	6	8	1.14	NHorOH> 5	Yes	1 alert: cathechol_A	Low	No
Pseudoceratine A *Marine sponge*	491.13	4	6	-0.47	None	Yes	0 alert	High	No
Frondoside A *Sea cucumber*	1335.43	10	29	-3.91	MW>500, NorO>10, NHorOH> 5	No	0 alert	Low	No

Visualization of 3D-Structures and Analyses of Interactions

To further elucidate the molecular docking results and visualize the key interactions between MNPs and the active sites of DDR related enzymes, BIOVIA Discovery Studio was employed for detailed interaction analyses (BIOVIA, 2021). Table 5 presents the top 10 most favorable MNPs for each DDRM receptor, ranked by the lowest BE, along with their predicted molecular interactions visualized, highlighting their hydrogen bonds and other interactions. The stability of ligand-receptor interactions is primarily governed by noncovalent interactions, among which is hydrogen bonds as it provides binding affinity (Adhav & Saikrishnan 2023), while hydrophobic contacts, van der Waals forces, and π-π stacking contribute to additional stabilization to enhance overall BE (Paik et al. 2022). In several complexes, hydrogen bonds found in the reference drugs were complemented or substituted by other interaction types, such as π-π stacking and electrostatic interactions, in the MNP complexes. This interchangeability of interaction types suggests that these noncovalent contacts are critical contributors to the favorable BE scores observed in the docking simulations (Hong et al. 2024).

In PARP-1 complexes, olaparib and talazoparib both formed two hydrogen bonds, stabilizing the drug-enzyme complex. Residues like TYR B:907 and HIS B:909 were repeatedly engaged in both positive controls and multiple MNPs such as Lamellarin R and Ningalin B, despite showing no hydrogen interactions. These catalytic residues may have contributed to ligand stabilization through other interactions such as van der Waals forces and π-π stacking. Consistent involvement of these residues among MNPs highlights their importance, suggesting that engagement may be sufficient to confer strong inhibitory potential even in the absence of classical hydrogen bonds (Liu et al. 2023). Moreover, the observed interaction patterns are consistent with previously reported structural and docking studies, thereby reinforcing the significance of specific amino acid residues in ligand binding. LYS B:903 was noted to be frequently involved in anchoring ligands within the PARP-1 active site, consistent with established interaction hotspots for potent PARP-1 inhibitors. This alignment supports the hypothesis that these residues serve as central mediators of strong ligand binding.

Although favorable interactions predominated in most complexes, certain ligand and receptor pairs, such as PARP-1_Ningalin B and TOPOI_Ulithiacyclamide B, revealed occasional unfavorable interactions. Nonetheless, these were outweighed by a greater number of stabilizing contacts, resulting in net negative or favorable BE. Across all receptor and ligand complexes, non-hydrogen bonding interactions were observed to contribute more significantly to the overall stability of the complexes than hydrogen bonds alone, underscoring the multifactorial nature of molecular binding. Notably, Lamellarin H has formed five hydrogen bonds, surpassing the controls in polar interactions, which might confer higher stability. This might indicate that certain MNPs could exceed the binding efficiency of clinical PARP-1 inhibitors.

In HDAC2, positive controls demonstrated strong but selected binding. Comparatively, Patellamide D and Ningalin B interacted with residues present in controls like PHE A:210, TYR A:209, and HIS A:183, which suggests that these compounds engage the enzyme through similar binding mechanisms as known inhibitors (Tateing and Suree 2022). Moreover, the recurring involvement of TYR A:308 in both our present study and the work of Liang et al. (2023) identifies this residue as a likely universal anchor across different inhibitory scaffolds. Presence of five hydrogen bonds can be observed in Patellamide B, indicating stronger binding than the controls, potentially enhancing stability. This may reinforce the potential of MNPs as alternative HDAC2 inhibitors given its diverse binding mechanisms and hydrogen bonds exceeding present drugs.

For TOPOI inhibitors, Topotecan exhibited four hydrogen bonds and 17 interactions, while Camptothecin, despite having no hydrogen bonds, has engaged in 16 residues, highlighting other interactions as major contributors to its binding stability. In comparison to controls, Lamellarin H and Lamellarin D have formed five and six hydrogen bonds, respectively. These MNPs have surpassed controls in polar contacts, particularly ASP A:533 and HIS A:367. The present results echo those of Boudjedir et al. (2021), who identified ARG A:364 as a key contact for stabilizing camptothecin-like molecules, primarily hydrogen bond formation. Their top performing compound achieved a BE of -229.993 kilocalories per mole, emphasizing the importance of this residue in promoting high affinity binding. This finding aligns with the TOPOI and Ulithiacyclamide B interactions observed in the current study wherein ARG A:364 formed a hydrogen bond. This convergence of findings strengthens the validity of the docking approach as it highlights the residue as a hotspot, reinforcing therapeutic potential.

TOPOII inhibitors such as Etoposide and Doxorubicin have exhibited three hydrogen bonds with around 16-20 residues with catalytic interactions such as ARG A:672, ARG A:727, and GLU A:839. Among the MNPs, Patellamide C and Patellamide A exhibited broader contact networks with interactions surpassing controls of 24 and 26 residues, respectively. This suggests that these compounds are anchored more deeply and tightly within the binding site compared to controls. The higher number of engaged residues reflects a more extensive active pocket, which can enhance stability and reduce likelihood of ligand dissociation (Wankowicz et al. 2022). Meanwhile, Ningalin has shown six hydrogen bonds, relying heavily on polar contacts on its stability.

Certain compounds displayed more selective binding preferences. TOPOI_Ulithiacyclamide B and TOPOII_Patellamide C each exhibited high affinity interactions, suggesting a more targeted inhibitory profile. This selectivity may prove advantageous in designing therapeutic strategies tailored to malignancies with specific dependencies on particular DDR pathways.

Table 5: Top 10 MNPs with lowest BE scores and their molecular interactions with DDRM-related receptors.

Target Receptor	Compound	Hydrogen Bonds	Other interactions
Positive Controls			
PARP-1	**Olaparib**	**2** ASP B:766 ARG B:878	**16** ALA B:880, ILE B:879, PRO B:881, LEU B:877, ILE B:872, ASP B:770, SER B:864, ASN B:868, ARG B:865, HIS B:909, GLY B:863, TYR B:907, HIS B:862, TYR B:896, TYR B:889, GLY B:888
PARP-1	**Talazoparib**	**2** ASN B: 868 ARG: 878	**16** ARG B:865, ASN B:767, ASP B:770, ASP B:878, ILE B:872, LEU B:877, GLY B:894, ILE B:895, HIS B:862, GLY B:863, TYR B:907, TYR B:896, TYR B:889, GLY B:888, GLU B:763, HIS B:909
HDAC2	**Panobinostat**	**1** HIS A: 183	**17** GLU A:208, GLN A:265, TYR A:209, LYS A:205, GLY A:305, HIS A:145, GLY A:306, ASP A:181, ASP A:269, HIS A:146, TYR A:308, CYS A:156, PHE A:155, PHE A:210, LEU A:276, GLY A:154, ASP A:104
HDAC2	**Vorinostat**	**1** LYS A:205	**7** ARG A:234, GLY A:207, TYR A:206, ASP A:235, GLU A:208, GLN A:358
TOPOI	**Topotecan**	**4** ARG A:364 HIS A:367 VAL A:502 ASN A:491	**17** LYS A:532, ARG A:488, ALA A:499, ASP A:533, THR A:498, PHE A:361, GLN A:421, GLY A:363, GLY A:365, SER A:534, LYS A:493, THR A:501, GLY A:531, GLY A:503, ALA A:489, GLY A:490, SER A:506
TOPOI	**Camptothecin**	**0**	**16** GLU A:356, LYS A:425, GLU A:418, LYS A:374, TRP A:416, PHE A:361, ILE A:420, ASN A:419, ARG A:375, ILE A:377, ILE A:355, ASN A:352, TYR A:352, TRP A:416, LYS A:354, ILE A:427
TOPOII	**Etoposide**	**3** ARG A:672 ARG A:727 GLU A:839	**20** LYS A:676, LYS A:827, ASP A:831, LEU A:829, ARG A:673, GLU A:712, LYS A:728, GLU A:837, PHE A:1003, PRO A:724, ILE A:715, LEU A:722, PRO A:716, LYS A:723, SER A:717, VAL A:1006, TRP A:840, ASP A:1004, HIS A:1005, GLY A: 1007
TOPOII	**Doxorubicin**	**3** ARG A:727 ARG A:673 ARG A:672	**16** LYS A:676, GLY A:1007, GLU A:712, PHE A:1003, SER A:717, GLU A:839, ILE A:715, PRO A:716, LEU A:722, LYS A: 723, LEU A:829, ASP A:831, LYS A:728, GLU A:837, PRO A:724, VAL A:836
Ligands			
PARP-1	**Ningalin B** *Marine sponge*	**0**	**23** TYR B:907, LYS B:903, GLU B:988, HIS B:909, ARG B:865,

			ASN B:767, ASN B:868, SER B:864, ASP B:766, TYR B:710, LEU B:769, PRO B:881, ARG B:878, ILE B:879, ALA B:880, GLY B:894, ILE B:895, HIS B:862, TYR B:896, GLY B:888, TYR B:889, MET B:890, LYS B:903
PARP-1	**Perophoramidine** *Sea squirt*	**0**	**21** ASP B:766, ARG B:865, ASN B:868, ASP B:770, SER B:864, ILE B:872, ARG B:878, LEU B:877, ILE B:895, GLY B:863, GLY B:894, SER B:904, HIS B:862, PHE B:897, TYR B:896, TYR B:907, GLY B:888, TYR B:889, ALA B:880, GLU B:763, HIS B:909
PARP-1	**Lamellarin R** *Marine sponge*	**0**	**25** GLU B:988, TYR B:907, GLY B:888, TYR B:889, MET B:890, TYR B:896, GLU B:763, HIS B:909, TYR B:689, ARG B:865, ASN B:767, ASN B:868, SER B:864, ASP B:766, ASP B:770, LEU B:769, PRO B:881, TYR B:710, GLY B:894, HIS B:862, ALA B:880, ILE B:872, LEU B:877, ILE B:875, ARG B:878
PARP-1	**Lamellarin O** *Marine sponge*	**2** ASP B:766 ARG B:865	**19** ALA B:880, ILE B:872, ARG B:878, LEU B:877, GLU B:988, GLY B:888, HIS B:862, TYR B:889, MET B:890, TYR B:907, TYR B:896, HIS B:909, GLU B:763, ASN B:767, ASN B:868, SER B:864, ASP B:770, LEU B:769, TYR B:710
PARP-1	**Lamellarin H** *Marine sponge*	**5** SER B:864 GLU B:763 TYR B:889 GLY B: 888 GLU B:988	**12** HIS B:909, GLN B:759, LYS B:903, TYR B:896, PHE B:897, TYR B:907, GLY B:863, HIS B:862, ASP B:766, ARG B:865, ASN B:868, ASN B:767
PARP-1	**Sansalvamide A** *Sea Squirt*	N/A	
PARP-1	**Ilimaquinone** *Marine Sponge*	**1** GLY B:863	**19** HIS B:862, ASP B:766, SER B:864, ASN B:868, ASP B:770, ARG B:878, LEU B:769, LEU B:877, ILE B:879, ALA B:880, GLY B:894, ILE B:895, TYR B:889, GLU B:988, LYS B:903, PHE B:897, TYR B:896, TYR B:907, SER B:904
PARP-1	**Pseudoceratine A** *Marine Sponge*	**4** ARG B:878 SER B: 864 ASN B: 868 ASP B: 766	**13** ILE B:872, ASP B:770, LEU B:769, TYR B:710, PRO B:881, TYR B:889, ILE B:879, ALA B:880, HIS B:862, TYR B:907, GLU B:763, HIS B:909, ARG B:865
PARP-1	**Lamellarin E** *Marine Sponge*	**4** ARG B:878 ASN B:868 TYR B:907 TYR B:896	**20** HIS B:909, ARG B:865, TYR B:889, LEU B:765, TYR B:710, ASP B:766, LEU B:769, ALA B:880, PRO B:881, ILE B:879, ASP B:770, LEU B:877, GLY B:894, HIS B:862, ILE B:895, GLN B:759, GLU B:763, ASN B:767, GLY B:888, SER B:864
PARP-1	**Diplosoma Ylidene-2** *Sea squirt*	**1** GLY B:863	**7** TYR B:889, GLY B:888, MET B:890, TYR B:896, TYR B:907, HIS B:862, SER B:864
HDAC2	**Perophoramidine** *Sea squirt*	**0**	**13** GLU A:208, TYR A:209, PHE A:155, TYR A:308, GLY A:154, HIS A:146, CYS A:156, GLY A:305, GLY A:306, GLN A:265, ASP A:269, PHE A:155, LEU A:276
HDAC2	**Frondoside A** *Sea cucumber*	N/A	
HDAC2	**Patellamide D** *Sea squirt*	**2** PHE A:210 HIS A:183	**12** TYR A:308, LEU A:276, GLU A:208, TYR A:209, PHE A:155, HIS A:146, GLY A:154, ASP A:104, HIS A:33, PRO A:34, ARG A:275, GLY A:32

HDAC2	**Ningalin B** *Marine sponge*	**3** ARG A: 275 TYR A: 308 PHE A: 210	**11** ASP A:104, PRO A:34, LEU A:276, GLY A:154, HIS A:146, ASP A:269, GLY A:306, HIS A:183, PHE A:155, TYR A:209, CYS A:278
HDAC2	**Lamellarin R** *Marine sponge*	**1** TYR A:209	**12** HIS A:183, TYR A:308, PHE A:210, HIS A:146, GLY A:154, PHE A:155, ASP A:104, LEU A:276, PRO A:34, ASP A:235, LYS A:205, CYS A:278
HDAC2	**Patellamide C** *Sea squirt*	**1** PHE A:210	**8** TYR A:209, GLU A:208, LEU A:276, ASP A:104, HIS A:183, GLY A:154, PHE A:155, HIS A:146
HDAC2	**Ulithiacyclamide B** *Sea squirt*	**0**	**12** CYS A:278, LEU A:276, PHE A:210, HIS A:183, PHE A:155, PRO A:34, ASP A:104, GLY A:154, GLU A:208, LYS A:205, ASP A:235, TYR A:209
HDAC2	**Patellamide A** *Sea squirt*	**0**	**13** GLU A:208, GLY A:277, ARG A:275, LYS A:205, CYS A:278, TYR A:209, PRO A:34, LEU A:276, ASP A:104, GLY A:154, PHE A:210, PHE A:155, HIS A:183
HDAC2	**Patellamide B** *Sea squirt*	**5** GLU A:190 PRO A:211 LYS A:148 SER A:153 GLU A:151	**8** ASP A:186, GLY A:212, THR A:213, PHE A:210, TYR A:193, THR A:194, GLU A:189, ASP A:218
HDAC2	**Didemnin B** *Sea squirt*	N/A	
TOPOI	**Didemnin B** *Sea squirt*	N/A	
TOPOI	**Ulithiacyclamide B** *Sea squirt*	**1** ARG A:364	**19** LYS A:532, SER A:506, PHE A:361, ASN A:491, ALA A:489, GLY A:503, THR A:498, GLN A:421, ARG A:488, SER A:423, GLY A:531, VAL A:502, THR A:501, ILE A:424, TYR A:426, LYS A:493, LYS A:425. ASP A:533, MET A:428
TOPOI	**Patellamide B** *Sea squirt*	**1** LYS A:532	**18** PTR A:723, ARG A:488, ARG A:590, LYS A:587, ALA A:586, THR A:585, ASN A:574, ASN A:491, LYS A:493, ALA A:489, THR A:498, ILE A:424, LYS A:425, TYR A:426, GLY A:490, GLY A:503, VAL A:502, THR A:501
TOPOI	**Patellamide C** *Sea squirt*	**1** LYS A:425	**18** GLY A:363, ARG A:364, LYS A:436, MET A:438, TYR A:426, ALA A:351, ILE A:427, ASN A:352, TRP A:416, ILE A:355, PRO A:358, LYS A:374, ARG A:375, ILE A:377, ASN A:419, GLU A:418, ILE A:420, GLU A:356
TOPOI	**Ningalin B** *Marine sponge*	**3** LYS A:374 TRP A:416 GLU A:356	**16** PHE A:361, GLY A:363, ARG A:362, LEU A:360, ARG A:364, PRO A:358, PRO A:357, ARG A:375, ILE A:377, GLU A:418, TYR A:426, ILE A:427, ASN A:352, LYS A:354, ILE A:355, LYS A:425
TOPOI	**Lamellarin H** *Marine sponge*	**5** ALA A:499 THR A:501 VAL A:502 LYS A:532 ARG A:364	**9** ASP A:533, GLY A:531, ARG A:488, GLY A:490, GLY A:503, HIS A:367, LYS A:493, THR A:498, SER A:534
TOPOI	**Patellamide A**	**3**	**18**

	Sea squirt	LYS A:425 ARG A:364 ASP A:533	TYR A:426, SER A:423, GLN A:421, ILE A:420, GLU A:418, PHE A:361, SER A:534, GLY A:365, ALA A:499, THR A:498, HIS A:367, LYS A:493, LYS A:532, ALA A:489, ARG A:488, ASN A:491, GLY A:490, ILE A:424
TOPOI	**Patellamide D** *Sea squirt*	**2** LYS A:425 GLN A:421	**17** GLY A:363, PHE A:361, HIS A:367, ASP A:533, ARG A:364, ALA A:499, GLY A:365, SER A:534, THR A:501, LYS A:532, THR A:498, ASN A:491, GLY A:492, LYS A:493, GLY A:497, GLY A:494, SER A:423
TOPOI	**Lamellarin D** *Marine sponge*	**6** HIS A:367 ASP A:533 SER A:534 ALA A:489 GLN A:421	**6** GLY A:363, ALA A:499, LYS A:532, THR A:501, LYS A:493, ASN A:491
TOPOI	**Frondoside A** *Sea cucumber*	N/A	
TOPOII	**Patellamide C** *Sea squirt*	**1** ASP A:831	**24** SER A:756, HIS A:758, ASP A:832, LEU A:592, GLU A:596, VAL A:836, LYS A:728, GLU A:837, LEU A:829, GLU A:839, PRO A:724, GLY A:1007, ARG A:727, GLU A:712, PHE A:1003, ILE A:715, LYS A:723, PRO A:716, SER A:717, ARG A:673, TRP A:840, LYS A:676, ARG A:672, LYS A:827
TOPOII	**Patellamide A** *Sea squirt*	**2** ASP A:831 ARG A:672	**26** GLU A:712, GLY A:1007, GLU A:839, PHE A:1003, LYS A:723, ILE A:715, ARG A:727, SER A:717, PRO A:724, GLU A:837, LEU A:829, LYS A:728, VAL A:836, SER A:755, SER A:756, ASP A:832, TYR A:757, HIS A:758, GLN A:544, LEU A:592, PRO A:593, GLU A:596, LYS A:599, LYS A:676, LYS A:827, ARG A:673
TOPOII	**Frondoside A** *Sea cucumber*	N/A	
TOPOII	**Ningalin B** *Marine sponge*	**6** LYS A:676 ARG A:673 LYS A:827 GLU A:837 LYS A:728 ARG A:727	**15** ARG A:672, GLU A:712, GLY A:1007, PHE A:1003, ILE A:715, LYS A:723, LEU A:722, PRO A:716, PRO A:724, SER A:717, TRP A:840, ASP A:831, LEU A:829, TYR A:830, GLU A:839
TOPOII	**Didemnin B** *Sea squirt*	N/A	
TOPOII	**Patellamide B** *Sea squirt*	**2** ARG A:672 GLU A:712	**21** LEU A:680, GLY A:679, LYS A:676, ASP A:831, GLU A:596, LEU A:592, GLU A:682, PRO A:593, GLU A:839, ARG A:727, TRP A:840, ARG A:673, VAL A:1006, GLY A:1007, LYS A:728, GLU A:837, LEU A:829, PRO A:724, GLN A:544, PRO A:681, ARG A:675
TOPOII	**Ulithiacyclamide B** *Sea squirt*	**5** SER A:763 TYR A:757 ILE A:856 ASN A:770 LYS A:723	**10** THR A:767, ARG A:713, SER A:714, HIS A:759, GLY A:855, MET A:762, GLY A:760, GLU A:854, ARG A:929, MET A:766
TOPOII	**Lamellarin O** *Marine sponge*	**2** LYS A:676 ARG A:673	**19** LEU A:680, GLU A:682, ARG A:675, ARG A:672, GLU A:712, LEU A:829, PRO A:724, LYS A:728, GLU A:837, ARG A:727, PRO A:838, GLU A:839, ASP A:1004, PHE A:1003, SER A:717, HIS A:1005, TRP A:840, GLU A:1007, VAL A:1006

TOPOII	**Lamellarin R** *Marine sponge*	**4** ASN A:770 ILE A:856 ASP A:545 TYR A:757	**10** SER A:714, GLY A:855, LYS A:489, HIS A:759, ARG A:713, SER A:763, GLY A:725, LYS A:723, THR A:767, GLN A:726
TOPOII	**Perophoramidine** *Sea squirt*	**1** GLU A:839	**17** ASP A:831, LYS A:827, LEU A:829, TRP A:840, LYS A:676, ARG A:673, VAL A:1006, ASN A:708, ARG A:672, GLY A:1007, ASP A:1004, PHE A:1003, SER A:717, PRO A:724, GLU A:712, ARG A:727, PRO A:838

From the top 10 most favorable complexes per receptor identified, top four complexes were prioritized that satisfied the criteria of lowest binding energies across their respective DDRM target and demonstrated favorable drug-likeness properties. These included PARP-1_Ningalin B, HDAC2_Perophoramidine, TOPOI_Ulithiacyclamide B, and TOPOII_Patellamide C, as illustrated in Figure 2, which shows the docked complexes and their significant binding interactions.

The 3D visualization and interaction analysis corroborated the docking results, highlighting both broad spectrum and selective inhibitory potential among the evaluated MNPs. In PARP-1_Ningalin B in Figure 2A, its aromatic alkaloid core and the presence of aromatic rings may facilitate π-π stacking interactions and hydrophobic contacts with key amino acid residues (Lanzarotti et al. 2020), while structural flexibility may enhance conformational adaptability within the active site. This interaction is consistent with its polyaromatic structure and reported activity as P-glycoprotein modulator, further supporting its potential as multitarget inhibitor. Additionally, the functional groups found in MNP scaffolds, including hydroxy, amino, and carbonyl moieties, may enhance molecular recognition via hydrogen bonding and electrostatic interactions (Paggi et al. 2024). This is especially notable in the HDAC2_Perophoramidine complex in Figure 2B, where multiple polar contacts and its indole nucleus may stabilize the binding conformation and contribute to its high affinity (Konyar et al. 2022). In TOPOI_Ulitithiacyclamide B complex (Figure 2C), its cyclic peptide backbone showed selective hydrogen bond networks that may account for its favorable binding and confers rigidity despite its size. While TOPOII_Patellamide C (Figure 2D) combines aromatic and hydrophobic residues that strengthens π-π stacking and van der Waals interactions that support conformational stability within its catalytic pocket.

Overall, aromatic rings, indole cores, and cyclic-peptide backbones emerge as common motifs in the high-affinity complexes. These features (π–π stacking, hydrogen-bonding groups) rationalize the observed binding strengths and can guide future optimization (Makwana and Mahalakshmi 2015). Notably, the four highlighted MNP–protein complexes combine strong binding with favorable drug-like properties, underscoring their translational potential.

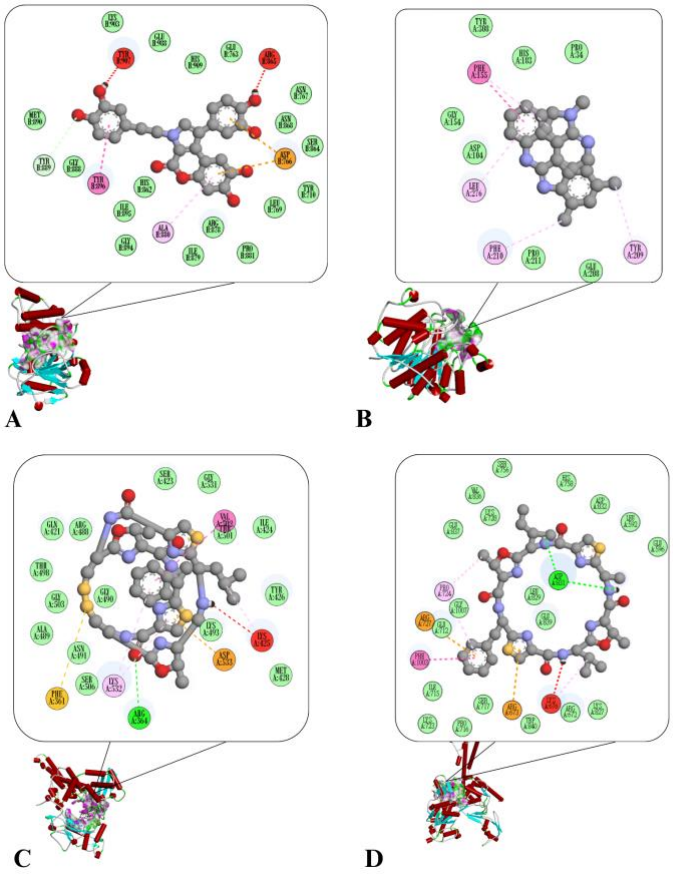

Figure 2(A-D): Visualization of docked complexes and their significant interactions. (**A**) PARP-1_Ningalin B, (**B**) HDAC2_Perophoramidine, (**C**) TOPOI_Ulithiacyclamide B, (**D**) TOPOII_Patellamide C. Interactions: light green - van der Waals, neon green - conventional hydrogen bond, pastel green - carbon hydrogen bond, orange - pi-anion, neon pink - π-π stacked, light pink - pi-alkyl, red – unfavorable.

Molecular Dynamics (MD) Simulations

MD simulations were conducted to assess the stability and interaction behavior of the top MNPs with DDRM-related targets. Key parameters analyzed included root mean square deviation (RMSD), root mean square fluctuations (RMSF), radius of gyration (Rg), and interaction energies.

Root Mean Square Deviation

RMSD analysis revealed the structural deviation of each complex over the 50 ns simulation period, providing insight into binding stability. Results are shown in Figure 3. Among the tested complexes, PARP-1_Ningalin B exhibited the greatest stability (lowest RMSD), suggesting the complex remains tightly bound throughout 50 ns. This suggests that once Ningalin B binds to PARP-1, it maintained a stable interaction that may contribute to enzyme inhibition (Malaluan et al. 2022). Similarly, HDAC2_Perophoramidine also showed low RMSD (~2–3 Å), consistent with reliable complex formation (Quimque et al. 2021). In contrast, TOPOI_Ulithiacyclamide B had high RMSD (8–12 Å), indicating structural mismatch, whereas TOPOII_Patellamide C remained stable.

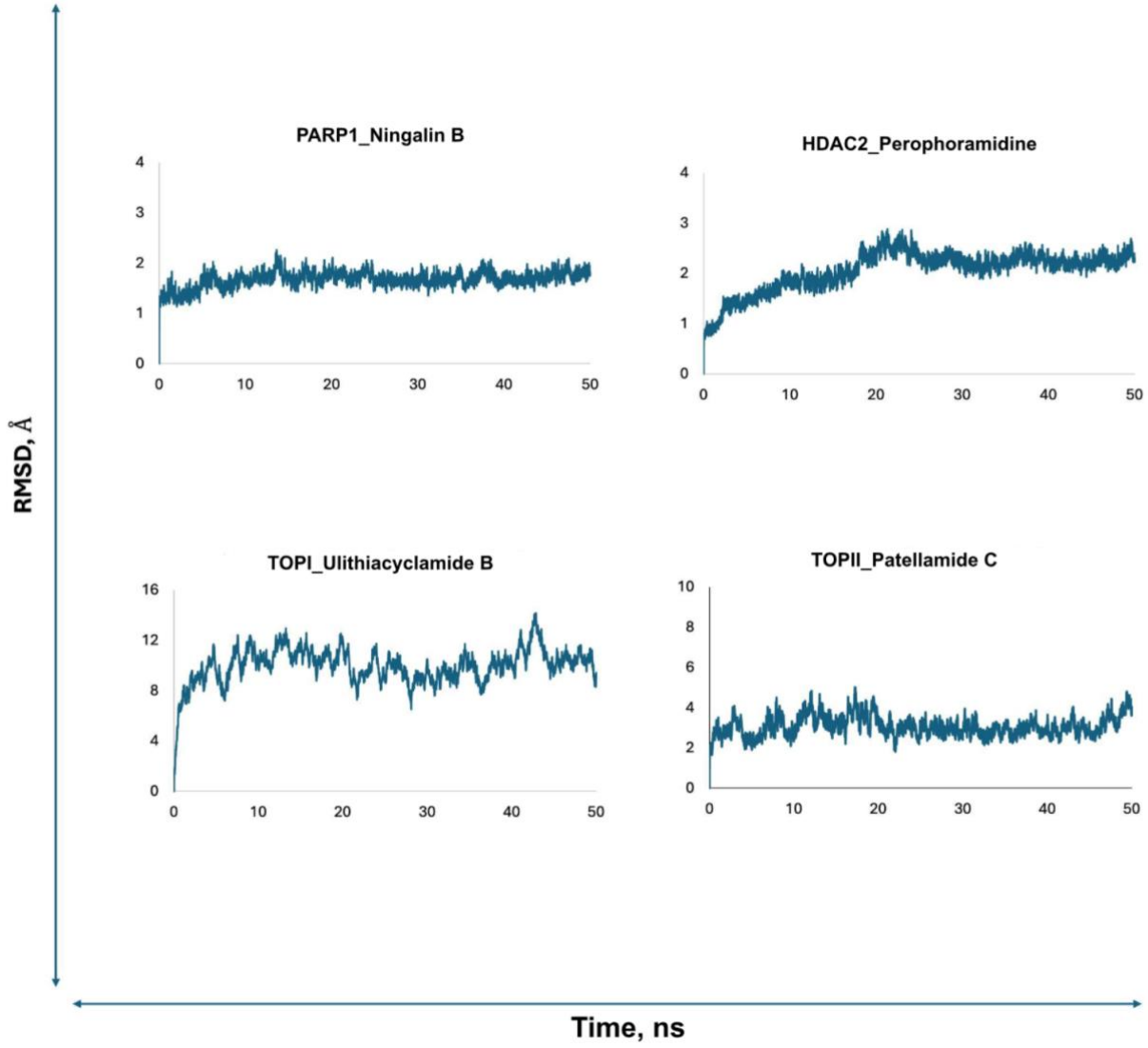

Figure 3: RMSD (Å) of top-scoring protein−ligand complexes as determined during 50 ns of MD simulation. The y-axis shows the RMSD value in Å while the x-axis shows the time in nanoseconds (ns).

Root Mean Square Fluctuations

RMSF analysis quantifies the displacement of individual atoms or residues from their average positions throughout the MD simulation, offering insight into residue-specific flexibility (Martínez 2015). The RMSF plots shown in Figure 4 revealed residue-specific flexibility across the four prioritized complexes. Because the PARP-1 (PDB ID: 4UND) and TOPOI (PDB ID: 1T8I) structures represent truncated catalytic domains, residue numbering in their RMSF plots reflects the original PDB sequence assignment rather than a continuous 1–n numbering.

The PARP-1–Ningalin B RMSF profile shows several localized peaks, indicating regions of flexibility; however, the overall profile suggests stable ligand binding. This implies that while localized conformational dynamics occur, they do not compromise complex stability, supporting the potential for structural rearrangements that may influence enzymatic inhibition (Manzano et al. 2022). Consistent with its flatter aromatic structure and strong docking score (–11.5 kcal/mol), Ningalin B appears to fit snugly within the binding site and stabilize surrounding residues.

The HDAC2–Perophoramidine complex exhibited a single dominant RMSF peak around residue 230, suggesting the presence of one flexible loop while the remainder of the enzyme structure remains relatively rigid. This limited fluctuation is indicative of higher structural stability and is consistent with the RMSD results (Luo et al. 2025).

For TOPOI–Ulithiacyclamide B, a dominant fluctuation peak was observed near residue 680, whereas the TOPOII–Patellamide C complex displayed a comparatively flatter RMSF

profile, indicative of greater overall stability. The presence of isolated flexible regions across these enzymes highlights a recurring pattern of localized conformational modulation, which may facilitate structural adaptation during interactions with DNA or other ligands and influence catalytic or regulatory functions (Narayanan et al. 2016; Hupfeld et al. 2024).

These findings suggest that the molecular plasticity observed in specific residues could be strategically targeted by MNPs. By binding to or near these flexible regions, MNPs may exploit structural vulnerabilities, inducing conformational shifts that destabilize the enzyme's active form (Childers and Daggett 2017; Crean et al. 2020). Such disruption has the potential to inhibit DNA repair, chromatin remodeling, and transcriptional regulation, ultimately compromising genomic integrity and cell survival (Damsma et al. 2013; Ishida et al. 2023). The RMSF results therefore provide mechanistic insight into how MNPs may exert inhibitory effects through modulation of residue-level flexibility across DDRM targets.

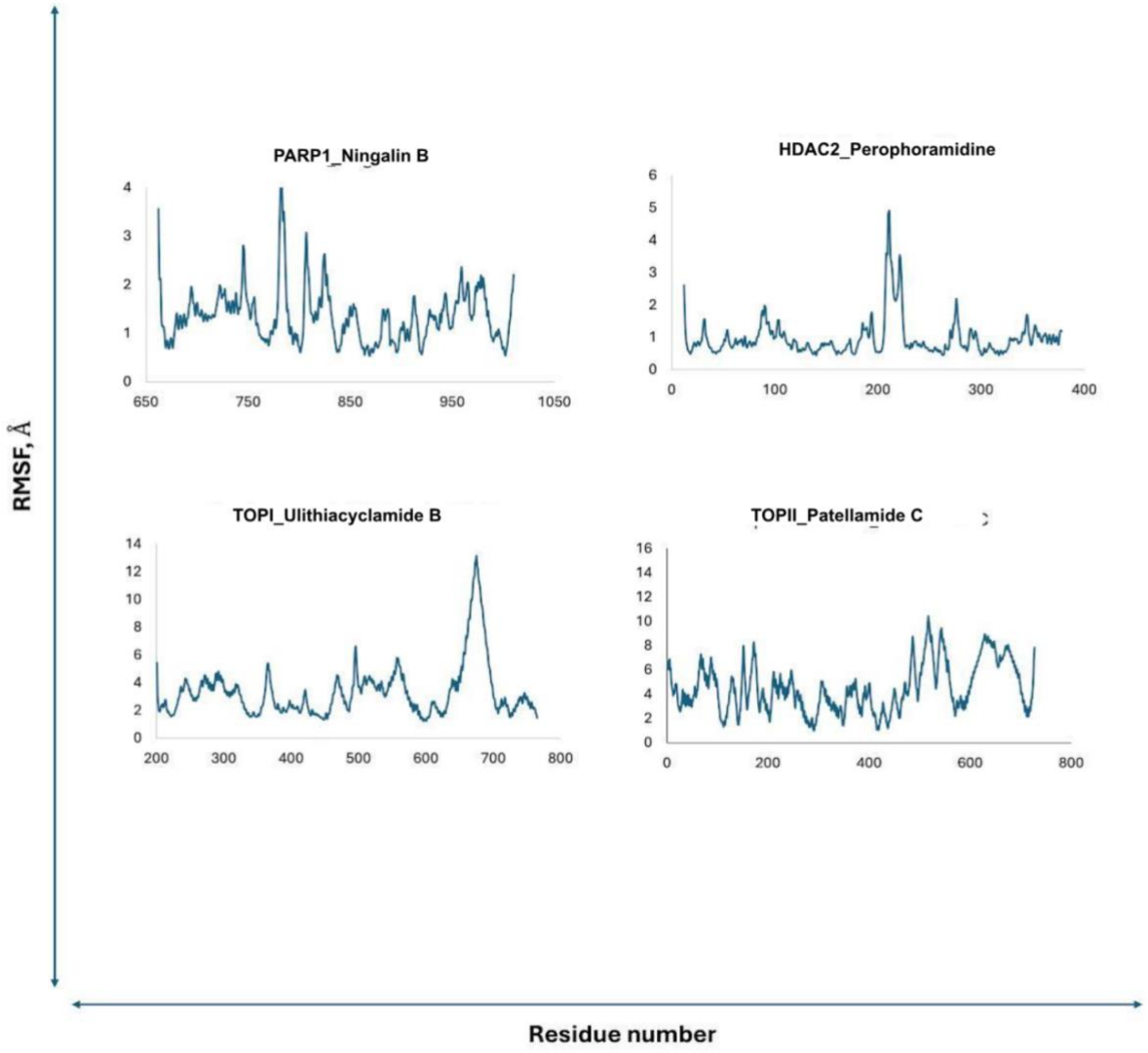

Figure 4: RMSF (Å) of top-scoring protein−ligand complexes as determined during 50 ns of MD simulation. The y-axis shows the RMSF value in Å while the x-axis shows the residue number.

Radii of Gyration

Rg provides a quantitative measure of the distribution of atoms around the center of mass of a molecule. It offers insight into the folding, compactness, and overall structural stability of the complex. Figure 5 shows that HDAC2 and PARP-1 complexes have lower Rg (more compact) than TOPOI/TOPOII complexes. This suggests PARP-1 and HDAC2 complexes are more compact and potentially more stable (Ghahremanian et al. 2022). The larger Rg values for the topoisomerases likely reflect their inherent conformational flexibility with DNA. These enzymes must undergo significant conformational changes during their catalytic cycle, and greater flexibility can be advantageous in this context. Despite the differences between enzyme types, all six complexes showed only minor variations in Rg values per compound, indicating consistent compactness across ligand interactions (Quimque et al. 2021).

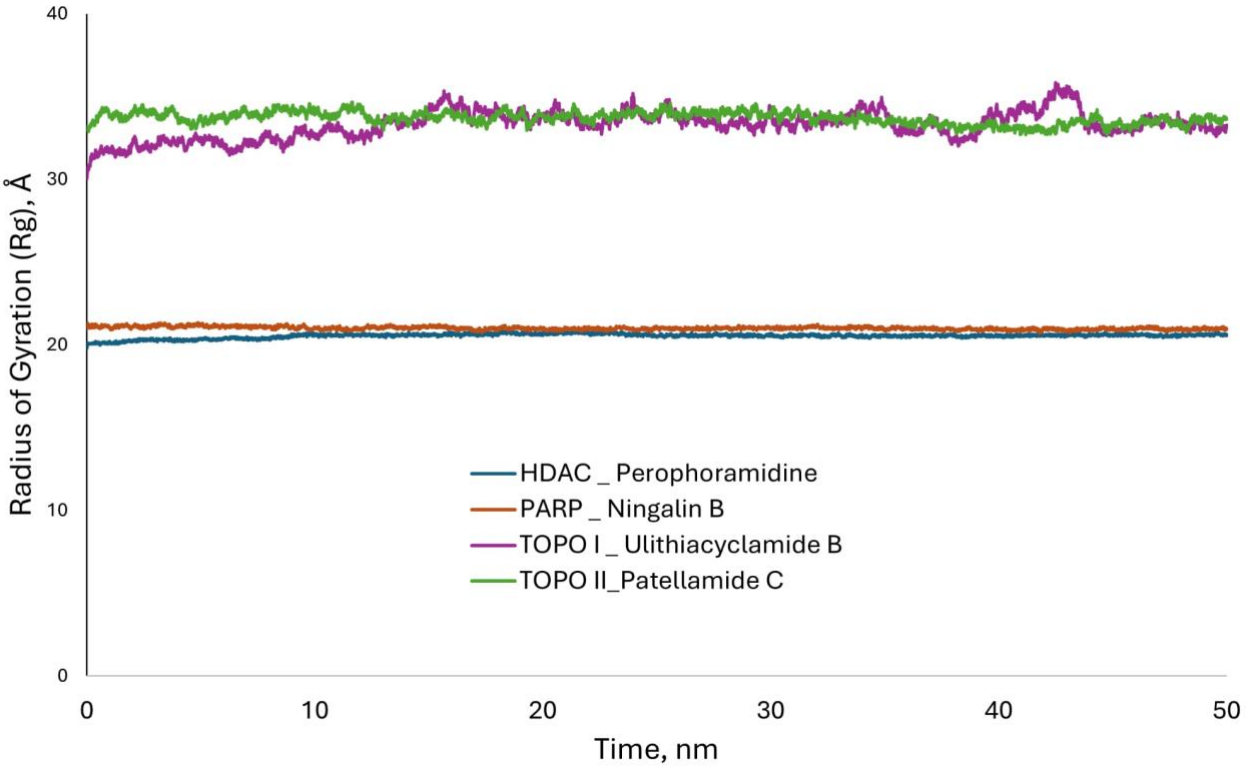

Figure 5: Summary of radii of gyration per time of the top-scoring complexes. The y-axis shows the Rg value in Å while the x-axis shows the time in nanoseconds (ns).

One limitation is the 50 ns simulation length, which may not capture long-term dynamics, especially for large enzymes. Additionally, we did not simulate controls (apo proteins or known inhibitors). Future studies should extend simulation time and include such controls for comparison.

Interaction Energies

The interaction energies of all enzyme-ligand complexes were assessed to evaluate their thermodynamic stability. The short-range Coulomb energy (Coulomb SR) describes electrostatic interactions between charged atoms, while the short-range Lennard-Jones energy (Lennard-Jones SR) models van der Waals and hydrophobic interactions between neutral atoms. All complexes had negative Coulomb and Lennard-Jones energies, indicating thermodynamically favorable binding (Manzano et al. 2022).

PARP-1–Ningalin B had the most negative total energy (–433.0 kcal/mol), indicating a particularly stable complex. This could induce inhibitory conformational changes in PARP-1. HDAC2–Perophoramidine (–66.1 kcal/mol), TOPOI–Ulithiacyclamide B (–155.4 kcal/mol), and TOPOII–Patellamide C (–215.1 kcal/mol) also had negative interaction energies, reflecting stable binding. The high magnitudes of Coulomb and LJ terms suggest many strong contacts

Overall, RMSD, RMSF, Rg, and interaction-energy profiles consistently indicated that the protein–ligand complexes remained stable during the simulations. Ningalin B stood out as a strong PARP-1 binder. These findings highlight the potential of the top MNPs to stabilize inactive conformations of DDR enzymes." Then briefly note missing analyses: "We note that hydrogen bond occupancy and detailed energetic decomposition were not performed; these will be addressed in future work.

Table 6: Average protein−ligand interaction energy from a 50 ns simulation trajectory of the top complexes

Complex	Energy Terms (kcal/mol)		
	Coulomb SR	Lennard-Jones SR	Interaction Energy
PARP-1_Ningalin B	-289.2850 ± 48.0920	-143.7610 ± 38.1991	-433.0460 ± 61.4167
HDAC2_Perophoramidine	-11.1483 ± 15.7181	-54.9490 ± 27.0152	-66.0973 ± 31.2550

TOPO I_Ulithiacyclamide B	-44.6974 ± 39.1783	-110.6710 ± 33.7433	-155.3684 ± 51.7064
TOPO II_Patellamide C	-41.5686 ± 36.3950	-173.4970 ± 20.3782	-215.0656 ± 41.7117

CONCLUSION

This computational study highlights selected Philippine MNPs as multitarget inhibitors of DDR enzymes (PARP-1, HDAC2, TOPOI, TOPOII). In particular, Ningalin B, Perophoramidine, Ulithiacyclamide B, and Patellamide C exhibited strong binding, favorable drug-like profiles, and stable MD interactions. Despite some Lipinski violations in larger compounds, proposed structural modifications and delivery strategies could enhance their druggability. These findings support the promise of MNPs as scaffolds for the development of novel anticancer agents capable of disrupting multiple pathways essential for genome maintenance and cell survival. However, these findings are based on computational models and must be validated experimentally. We did not perform comprehensive *in vitro* or *in vivo* pharmacokinetic or toxicity tests, which are necessary next steps. Future work should include cytotoxicity assays in cancer cell lines and in vivo studies in animal models to assess efficacy and safety. Our results represent an early phase in drug discovery. Significant additional preclinical development (optimization, formulation, trials) will be needed before any clinical use. Despite being a preliminary step, our favorable *in silico r*esults underscore the promise of these natural-product scaffolds for anticancer drug development.

ACKNOWLEDGMENTS

The authors acknowledge Dr. Lemmuel Tayo of the Mapua University for his inputs in the project.

CONFLICT OF INTEREST

The authors declare that there is no conflict of interest.

CONTRIBUTIONS OF INDIVIDUAL AUTHORS

C.M.S. conceptualized the research study. J.L.R. led the study design. F.B.S., J.S., J.L.R., and C.M.S. performed literature search and data collection. J.L.R., J.A.H.M., and E.B.R. developed the methodology. J.L.R., J.S., F.B.S., M.T.J.Q., J.C.M.A., and J.A.H.M. conducted the experimentation and data visualization. F.D.B., J.L.R., C.M.S., J.S., and J.A.H.M. collaboratively finalized, examined, and analyzed the overall data and results to ensure accuracy and consistency. F.D.B., J.L.R., C.M.S., J.S., E.B.R., M.T.J.Q., C.J.M.A., J.A.H.M., and C.J.L. contributed to writing, editing, and refining the manuscript. J.A.H.M. and C.J.L. provided supervision and finalized the manuscript. All authors read and approved the final manuscript.

REFERENCES

Abraham M, Alekseenko A, Andrews B, Basov V, Bauer P, Bird H, Briand E, Brown A, Doijade M, Fiorin G, Fleischmann S, Gorelov S, Gouaillardet G, Gray A, Irrgang ME, Jalalypour E, Johansson P, Kutzner C, Lazarski G, Lemkul JA, Lundborg M, Merz P, Miletić V, Morozov D, Müllender L, Nabet J, Páll S, Pasquadibisceglie A, Pellegrino M, Piasentin N, Rapetti D, Sadiq MU, Santuz H, Schulz R, Shirts M, Shugaeva T, Shvetsov A, Turner P, Villa A, Wingbermühle S, Hess B, Lindahl E. GROMACS 2025.3 Manual. Zenodo 2017. https://doi.org/10.5281/zenodo.16992569.

Adhav VA, Saikrishnan K. The realm of unconventional noncovalent interactions in proteins: their significance in structure and function. ACS Omega 2023: 8(25), 22268–22284. https://doi.org/10.1021/acsomega.3c00205

Adrian TE, Collin P. The Anti-Cancer Effects of Frondoside A. Marine drugs 2018: 16(2), 64. https://doi.org/10.3390/md16020064

Acyatan Z, Susana-Guevarra S, Picart MR, Belen E, Salvador-Reyes L, Concepcion G. In vivo anti-tumor and anti-metastatic activity of renieramycin M and doxorubicin combination treatments on 4T1 breast cancer murine model. SciEnggJ 2024: 17(Supplement), 379–390. https://doi.org/10.54645/202417supnlt-14

Ahmed S, Alam W, Jeandet P, Aschner M, Alsharif KF, Saso L, Khan H. Therapeutic Potential of Marine Peptides in Prostate Cancer: Mechanistic Insights. Marine drugs 2022: 20(8), 466. https://doi.org/10.3390/md20080466

Al-Asif A, Kamal AHM, Hamli H, Idris MH, Gerusu GJ, Ismail J, Bhuiyan MKA, Abualreesh MH, Musa N, Abd Wahid ME, Mishra M. Status, biodiversity, and ecosystem services of seagrass habitats within the Coral Triangle in the Western Pacific Ocean. Ocean Science Journal 2022: 57(2), 147–173. https://doi.org/10.1007/s12601-022-00068-w

Bailly C. Anticancer properties of lamellarins. Marine drugs 2015: 13(3), 1105–1123. https://doi.org/10.3390/md13031105

Baker NM, Rajan R, Mondragón A. Structural studies of type I topoisomerases. Nucleic Acids Research 2009: 37(3), 693–701. https://doi.org/10.1093/nar/gkn1009

Bitew M, Desalegn T, Demissie TB, Belayneh A, Endale M, Eswaramoorthy R. Pharmacokinetics and drug-likeness of antidiabetic flavonoids: Molecular docking and DFT study. PLOS ONE 2021: 16(12), e0260853. https://doi.org/10.1371/journal.pone.0260853

BIOVIA, Dassault Systèmes, Discovery Studio, 2021, San Diego: Dassault Systèmes, 2021.

Boudjedir A, Kraim K, Saihi Y, Attoui-Yahia O, Ferkous F, Khorief Nacereddine A. A computational molecular docking study of camptothecin similars as inhibitors for topoisomerase 1. Structural Chemistry 2021: 32(2), 689–697. https://doi.org/10.1007/s11224-020-01633-6

Bressi JC, Jennings AJ, Skene R, Wu Y, Melkus R, De Jong R, O'Connell S, Grimshaw CE, Navre M, Gangloff AR. Exploration of the HDAC2 foot pocket: Synthesis and SAR of substituted N-(2-aminophenyl) benzamides. Bioorganic & Medicinal Chemistry Letters 2010: 20(10), 3142–3145. https://doi.org/10.1016/j.bmcl.2010.04.020

Childers MC, Daggett V. Insights from molecular dynamics simulations for computational protein design. Molecular Systems Design & Engineering 2017: 2(1), 9-33. https://doi.org/10.1039/C6ME00083E

Chatterjee N, Walker GC. Mechanisms of DNA damage, repair, and mutagenesis. Environmental and Molecular Mutagenesis 2017: 58(5), 235–263. https://doi.org/10.1002/em.22087

Chen L, Hu JS, Xu JL, Shao CL, Wang GY. Biological and chemical diversity of ascidian-associated microorganisms. Marine Drugs 2018: 16(10), 362. https://doi.org/10.3390/md16100362

Cheng B, Pan W, Xing Y, Xiao Y, Chen J, Xu Z. Recent advances in DDR (DNA damage response) inhibitors for cancer therapy. European Journal of Medicinal Chemistry 2022: 230, 114109. https://doi.org/10.1016/j.ejmech.2022.114109

Coimbra JTS, Feghali R, Ribeiro RPPL, Ramos MJ, Fernandes PA. The importance of intramolecular hydrogen bonds on the translocation of the small drug piracetam through a lipid bilayer. RSC Advances 2021: 11(2), 899–908. https://doi.org/10.1039/D0RA09995C

Concepcion GP, Anas ARJ, Azcuna MA. Anticancer compounds from Philippine marine organisms act on major pathways in cancer. Philippine Science Letters 2014: 7(1), 207–227. https://scienggj.org/2014/PSL%202014-vol07-no01-p207-227%20Azcuna.pdf

Daina A, Michielin O, Zoete V. SwissADME: a free web tool to evaluate pharmacokinetics, drug-likeness and medicinal chemistry friendliness of small molecules. Scientific Reports 2017: 7(1), 42717. https://doi.org/10.1038/s41598-017-01825-8

Dantzic D, Noel P, Merien F, Liu DX, Lu J, Han H, McKeage MJ, Li Y. The Effects of Synthetically Modified Natural Compounds on ABC Transporters. Pharmaceutics 2018: 10(3), 127. https://doi.org/10.3390/pharmaceutics10030127

Damsma GE, Brown CJ, Darst SA. Mechanism of transcriptional regulation by TFIIS and its implications for RNA polymerase II backtracking. Nature Structural & Molecular Biology 2013: 20(3), 343–349.

De Leo V, Maurelli AM, Giotta L, Catucci L. Liposomes containing nanoparticles: preparation and applications. Colloids and Surfaces B: Biointerfaces 2022: 218, 112737. https://doi.org/10.1016/j.colsurfb.2022.112737

Eberhardt J, Santos-MArtins D, Tillack AF, Forli S. AutoDock Vina 1.2.0: New Docking Methods, Expanded Force Field, and Python Bindings. Journal of Chemical Information and Modeling 2021.

Fernandez RAT, Quimque MTJ, Notarte KI, Manzano JA, Pilapil DYH, de Leon VN, San Jose JJP, Villalobos O, Muralidharan NH, Gromiha MM, Brogi S, Macabeo APG. Myxobacterial depsipeptide chondramides interrupt SARS-CoV-2 entry by targeting its broad, cell tropic spike protein. Journal of Biomolecular Structure and Dynamics 2021. https://doi.org/10.1080/07391102.2021.1969281

Ghahremanian S, Rashidi MM, Raeisi K, Toghraie D. Molecular dynamics simulation approach for discovering potential inhibitors against SARS-CoV-2: A structural review. Journal of Molecular Liquids 2022: 354, 118901. https://doi.org/10.1016/j.molliq.2022.118901

Gomez MC, Alvarico RAD, Valbuena RE, Aquino AMC, Matira AR, Tayo LL. In silico protein structure comparison of conotoxins with VI/VII cysteine framework. Proceedings of the 2019 3rd International Conference on Computational Biology and Bioinformatics 2019: 1–6. https://doi.org/10.1145/3365966.3365978

Guha S, El-Deeb IY, Yadav S, Das R, Dutta Dubey K, Baruah M, Gremaud L, Sen S. Capturing a pentacyclic fragment-based library derived from perophoramidine: Their design, synthesis and evaluation as anticancer compounds by DNA double-strand breaks (DSB) and PARP-1 inhibition. Chemistry – A European Journal 2022: 28(63), 112085. https://doi.org/10.1002/chem.202202405

Hanwell MD, Curtis DE, Lonie DC, Vandermeersch T, Zurek E, Hutchison GR. Avogadro: An advanced semantic chemical editor, visualization, and analysis platform. Journal of Cheminformatics 2012, 4:17. https://doi.org/10.1186/1758-2946-4-17

Hetherington AM, Sawyez CG, Sutherland BG, Robson DL, Arya R, Kelly K, Jacobs RL, Borradaile, NM. Treatment with didemnin B, an elongation factor 1A inhibitor, improves hepatic lipotoxicity in obese mice. Physiological report 2016: 4(17), e12963. https://doi.org/10.14814/phy2.12963

Hong Y, Ha J, Sim J, Lim C, Oh K, Chandrasekaran R, Kim B, Choi J, Ko J, Shin W, Lee J. Accurate prediction of protein–ligand interactions by combining physical energy functions and graph-neural networks. Journal of Cheminformatics 2024: 16(1), 121. https://doi.org/10.1186/s13321-024-00912-2

Hopkins TA, Ainsworth WB, Ellis PA, Donawho CK, DiGiammarino EL, Panchal SC, Abraham VC, Algire MA, Shi Y, Olson AM, Johnson EF, Wilsbacher JL, Maag D. PARP1 trapping by PARP inhibitors drives cytotoxicity in both cancer cells and healthy bone marrow. Molecular Cancer Research 2019: 17(2), 409–419. https://doi.org/10.1158/1541-7786.MCR-18-0138

Huang C, Yang Z, Couch G, Meng E, Pettersen E, Goddard T. UCSF Chimera(Version 1.17.3) [Software]. University of California, San Francisco 2018. https://www.rbvi.ucsf.edu/chimera

Hupfeld E, Schlee S, Wurm JP, Rajendran C, Yehorova D, Vos E, Ravindra D, Kamerlin S, Sprangers R, Sterner R. Conformational modulation of a mobile loop controls catalysis in the (βα)8-barrel enzyme of histidine biosynthesis HisF. JACS 2024: 4(8), 3258–3276. https://doi.org/10.1021/jacsau.4c00558

Ibana FV, Von Novi O, Manzano JAH, Castillo AL, Macabeo APG. Alkenylated phenolics from *Syzygium lineatum* with antiproliferative activity against chronic myeloid leukemia cells. Journal of Applied Pharmaceutical Science 2024: 14(8), 070-077. https://doi.org/10.7324/JAPS.2024.170186

Ishida T, Takemoto Y. Synthetic study of perophoramidine: construction of pentacyclic core structure via SmI2-mediated reductive cyclization. Tetrahedron 2013: 69(23) 4517–4523). https://doi.org/10.1016/j.tet.2013.04.039

Ishida H, Matsumoto A, Tanaka H, Okuda A, Morishima K, Wade, PA, Kurumizaka H, Sugiyama M, Kono H. Structural and dynamic changes of nucleosome upon GATA3 binding. Journal of Molecular Biology 2023: 435(23), 168308. https://doi.org/10.1016/j.jmb.2023.168308

Jo H, Shim K, Kim HU, Jung HS. Jeoung D. HDAC2 as a target for developing anti-cancer drugs. Computational and Structural Biotechnology Journal 2023: 21, 2048–2057. https://doi.org/10.1016/j.csbj.2023.03.016

Karami TK, Hailu S, Feng S, Graham R, Gukasyan HJ. Eyes on Lipinski's Rule of Five: A New "Rule of Thumb" for Physicochemical Design Space of Ophthalmic Drugs. Journal of Ocular Pharmacology and Therapeutics 2022: 38(1), 43–55. https://doi.org/10.1089/jop.2021.0069

Karim F, Putra MY, Hadi TA, Abrar M. Antimicrobial and cytotoxic properties of the ascidians *Lissoclinum patella, Oxycoryna fascicularis, Didemnum molle, and Botryllus schlosseri.* Pharmaceutical Sciences and Research 2018: 5(2), 65–71. https://doi.org/10.7454/psr.v5i2.4137

Kathawala RJ, Gupta P, Ashby CR, Chen ZS. The modulation of ABC transporter-mediated multidrug resistance in cancer: a review of the past decade. Drug Resistance Updates 2015: 18, 1–17. https://doi.org/10.1016/j.drup.2014.11.002

Kenny P. Hydrogen-bond donors in drug design. Journal of Medicinal Chemistry 2022: 65(21). https://doi.org/10.1021/acs.jmedchem.2c01147

Konyar D, Okur H, Arslan Z. Molecular docking studies of cox inhibitors on wild-type ras. Journal of Faculty of Pharmacy of Ankara University 2022: 46(1), 23–34.

Kwak CH, Jin L, Han JH, Han CW, Kim E, Cho M, Chung TW, Bae SJ, Jang SB, Ha KT. Ilimaquinone Induces the Apoptotic Cell Death of Cancer Cells by Reducing Pyruvate Dehydrogenase Kinase 1 Activity. International Journal of Molecular Sciences 2020: 21(17), 6021. https://doi.org/10.3390/ijms21176021

Lanzarotti E, Defelipe LA, Marti MA, Turjanski AG. Aromatic clusters in protein–protein and protein–drug complexes. Journal of Cheminformatics 2020: 12(1), 30. https://doi.org/10.1186/s13321-020-00437-4

Lee J, Currano JN, Carroll PJ, Joullié MM. Didemnins, tamandarins and related natural products. Natural Product Reports 2012: 29(4), 404–424. https://doi.org/10.1039/C2NP00065B

Li W, Sun Z. Mechanism of action for HDAC inhibitors—Insights from omics approaches. International Journal of Molecular Sciences 2019: 20(7), 1616. https://doi.org/10.3390/ijms20071616

Liang S, Geng Y, Niu M-M, Zhang Y, He W, Li J, Yang L, Xu Z. Discovery and biological evaluation of novel CARM1/HDAC2 dual-targeting inhibitors with anti-prostate cancer agents. Journal of Enzyme Inhibition and Medicinal Chemistry 2023: 8(1), Article 2241118. https://doi.org/10.1080/14756366.2023.2241118

Liu F, Chen J, Li X, Liu R, Zhang Y, Gao C, Shi D. Advances in development of selective antitumor inhibitors that target PARP-1. Journal of Medicinal Chemistry 2023: 66(24), 16464–16483. https://doi.org/10.1021/acs.jmedchem.3c00865

Longakit MBA, Sotto FB, Kelly M. The shallow water marine sponges (Porifera) of Cebu, Philippines. Science Diliman 2005: 17(2), 52–74.

Luo H, Ma Y, Su Z, Gu Y, Zhang S, Gerstweiler L. Investigating the stability of chimeric murine polyomavirus VP1 capsomeres via molecular dynamics simulations and experimental analysis. International Journal of Biological Macromolecules 2025: 286, 138372. https://doi.org/10.1016/j.ijbiomac.2024.138372

Magalhães PR, Reis PB, Vila-Viçosa D, Machuqueiro M, Victor BL. Identification of Pan-Assay Interference compoundS (PAINS) Using an MD-Based Protocol. Methods Mol Biol 2021: 2315. 236-271. https://doi.org/10.1007/978-1-0716-1468-6_15. PMID: 34302681.

Magpantay HD, Malaluan IN, Manzano JA, Quimque MT, Pueblos KR, Moor N, Budde S, Bangcaya PS, Lim-Valle D, Dahse HM, Khan A, Wei DQ, Alejandro GJD, Macabeo AP. Antibacterial and COX-2 inhibitory tetrahydrobisbenzylisoquinoline alkaloids from the Philippine medicinal plant *Phaeanthus ophthalmicus*. Plants 2021: 10(3), 462. https://doi.org/10.3390/plants10030462

Makwana KM, Mahalakshmi R. Implications of aromatic–aromatic interactions: From protein structures to peptide models. Protein Science 2015: 24(12):1920-1933. https://doi.org/10.1002/pro.2814

Malaluan IN, Manzano JAH, Muñoz JER, Bautista TJL, Dahse HM, Quimque MTJ, Macabeo APG. Antituberculosis and Antiproliferative Activities of the Extracts and Tetrahydrobisbenzylisoquinoline Alkaloids from *Phaeanthus ophthalmicus: In Vitro* and *In Silico* Investigations. Philippine Journal of Science 2022: 151(1). https://doi.org/10.56899/151.01.28

Manzano JA, Abellanosa EA, Aguilar JP, Brogi S, Yen CH, Macabeo AP, Austriaco N. Globospiramine from *Voacanga globosa* exerts robust cytotoxic and antiproliferative activities on cancer cells by inducing caspase-dependent apoptosis in A549 cells and inhibiting MAPK14 (p38α): *in vitro* and computational investigations. Cells 2024a: 13(9), 772. https://doi.org/10.3390/cells13090772

Manzano JAH, Parico RARAD, Fabrique PJR, Maldupana AN, Arevalo JC, Agbay JCM, Quimque MT, Macabeo, APG. Multitargeting inhibitory activity of *Moringa oleifera* natural plant product scaffolds against proteins implicated in chronic myeloid leukemia: insights from molecular docking, molecular dynamics and ADMET predictions. Journal of Computational Biophysics and Chemistry 2025: 1-16. https://doi.org/10.1142/S273741652650033X

Manzano JA, Brogi S, Calderone V, Macabeo AP, Austriaco N. Globospiramine exhibits inhibitory and fungicidal effects against *Candida albicans* via apoptotic mechanisms. Biomolecules 2024b: 14(6), 610. https://doi.org/10.3390/biom14060610

Manzano JA, Cruz CL, Quimque MT, Macabeo AP. In silico potentials of *Alpinia galanga* constituents against human placental aromatase vital in postmenopausal estrogen-dependent breast cancer pathogenesis. Philippine Journal of Science 2022: 151(6A).

Manzano JA, Llames LC, Macabeo AP. Tetrahydrobisbenzylisoquinoline alkaloids from *Phaeanthus ophthalmicus* inhibit target enzymes associated with type 2 diabetes and obesity. Journal of Applied Pharmaceutical Science 2024: 14(1), 230-237. https://doi.org/10.7324/JAPS.2023.154518

Martínez L. Automatic identification of mobile and rigid substructures in molecular dynamics simulations and fractional structural fluctuation analysis. PLOS ONE 2015: 10(3), e0119264. https://doi.org/10.1371/journal.pone.0119264

McClendon AK, Osheroff N. DNA topoisomerase II, genotoxicity, and cancer. Mutation Research 2007: 623(1-2), 83–97. https://doi.org/10.1016/j.mrfmmm.2007.06.009

Mokhlesi A, Stuhldreier F, Wex KW, Berscheid A, Hartmann R, Rehberg N, Sureechatchaiyan P, Chaidir C, Kassack MU, Kalscheuer R, Brötz-Oesterhelt H, Wesselborg S, Stork B, Daletos G, Proksch P. Cyclic Cystine-Bridged Peptides from the Marine Sponge *Clathria basilana* Induce Apoptosis in Tumor Cells and Depolarize the Bacterial Cytoplasmic Membrane. Journal of natural products 2017: 80(11), 2941–2952. https://doi.org/10.1021/acs.jnatprod.7b00477

Molinski TF, Dalisay DS, Lievens SL, Saludes JP. Drug development from marine natural products. Nature Reviews Drug Discovery 2009: 8(1), 69–85. https://doi.org/10.1038/nrd2487

Narayanan C, Bernard DN, Doucet N. Role of conformational motions in enzyme function: Selected methodologies and case studies. Catalysts 2016: 6(6), 81. https://doi.org/10.3390/catal6060081

Newman DJ, Cragg GM. Natural products as sources of new drugs over the nearly four decades from 01/1981 to 09/2019. Journal of Natural Products 2020: 83(3), 770–803. https://doi.org/10.1021/acs.jnatprod.9b01285

Ogi T, Taira J, Margiastuti P, Ueda K. Cytotoxic metabolites from the Okinawan ascidian *Diplosoma virens. M*olecules 2008: 13(3), 595–602. https://doi.org/10.3390/molecules13030595

Paik D, Lee H, Kim H, Choi JM. Thermodynamics of π–π interactions of benzene and phenol in water. International Journal of Molecular Sciences 2022: 23(17), 9811. https://doi.org/10.3390/ijms23179811

Palanisamy SK, Rajendran NM, Marino A. Natural products diversity of marine ascidians (Tunicates; Ascidiacea) and successful drugs in clinical development. Natural Products and Bioprospecting 2017: 7(1), 1–111. https://doi.org/10.1007/s13659-016-0115-5

Paggi JM, Pandit A, Dror RO. (2024). The art and science of molecular docking. Annual Review of Biochemistry 2024: 93(1), 389–410. https://doi.org/10.1146/annurev-biochem-030222-120000

Peng X, Pan W, Jiang F, Chen W, Qi Z, Peng W, Chen J. Selective PARP1 inhibitors, PARP1-based dual-target inhibitors, PROTAC PARP1 degraders, and prodrugs of PARP1 inhibitors for cancer therapy. Pharmacological Research 2022: 186, 106529. https://doi.org/10.1016/j.phrs.2022.106529

Perilla JR, Goh BC, Cassidy CK, Liu B, Bernardi RC, Rudack T, Yu H, Wu Z, Schulten K. (2015). Molecular dynamics simulations of large macromolecular complexes. Current Opinion in Structural Biology 2015: 31, 64–74. https://doi.org/10.1016/j.sbi.2015.03.007

Pommier Y. Topoisomerase I inhibitors: camptothecins and beyond. Nature reviews. Cancer 2006: 6(10), 789–802. https://doi.org/10.1038/nrc1977

Pommier Y. DNA topoisomerase I inhibitors: Chemistry, biology and interfacial inhibition. Chemical Reviews 2009: 109(7), 2894–2902. https://doi.org/10.1021/cr900097c

Quimque MT, Notarte K, Fernandez RA, Manzano J, Yñigo DH, de Leon V, San Jose J, Villalobos O, Muralidharan N, Gromiha M, Brogi S, Macabeo APG. Virtual screening-driven drug discovery of SARS-CoV2 enzyme inhibitors targeting viral attachment, replication, post-translational modification and host immunity evasion infection mechanisms. Journal of Biomolecular Structure and Dynamics 2021. https://doi.org/10.1080/07391102.2021.1967286

Ramadhani D, Maharani R, Gazzali AM, Muchtaridi M. Cyclic Peptides for the Treatment of Cancers: A Review. Molecules 2022: 27(14), 4428. https://doi.org/10.3390/molecules27144428

Sajwani FH. Frondoside A is a potential anticancer agent from sea cucumbers. Journal of Cancer Research and Therapeutics 2019: 15(5), 953–960. https://doi.org/10.4103/jcrt.JCRT_1427_16

Shenkar N, Swalla BJ. Global diversity of Ascidiacea. PLoS One 2011: 6(6), e20657. https://doi.org/10.1371/journal.pone.0020657

Schmidt EW, Nelson JT, Rasko DA, Sudek S, Eisen JA, Haygood MG, Ravel J. Patellamide A and C biosynthesis by a microcin-like pathway in *Prochloron didemni,* the cyanobacterial symbiont of *Lissoclinum patella*. Proceedings of the National Academy of Sciences 2005: 102(20), 7315–7320. https://doi.org/10.1073/pnas.0501424102

Staker BL, Feese MD, Cushman M, Pommier Y, Zembower D, Stewart L, Burgin AB. Structures of three classes of anticancer agents bound to the human topoisomerase I− DNA covalent complex. Journal of Medicinal Chemistry 2005: 48(7), 2336-2345. https://doi.org/10.1021/jm049146p

Seto E, Yoshida M(2014). Erasers of histone acetylation: the histone deacetylase enzymes. Cold Spring Harbor perspectives in biology 2014: 6(4), a018713. https://doi.org/10.1101/cshperspect.a018713

Tan MA, Manzano JA, Ishikawa H. Amyloid-beta aggregation and advanced glycation end-products inhibitory activities of *Pandanus amaryllifolius* Roxb. alkaloids: insights from in vitro and computational investigations. Chemical Papers 2024: 78(18):9359-9367. https://doi.org/10.1007/s11696-024-03747-1

Tateing S, Suree N. Decoding molecular recognition of inhibitors targeting HDAC2 via molecular dynamics simulations and configurational entropy estimation. PLoS One 2022: 17(8), e0273265. https://doi.org/10.1371/journal.pone.0273265

Thorsell AG, Ekblad T, Karlberg T, Low M, Pinto AF, Trésaugues L, Moche M, Cohen MS, Schuler H. Structural basis for potency and promiscuity in poly(ADP-ribose) polymerase (PARP) and tankyrase inhibitors. Journal of Medicinal Chemistry 2017: 60(4), 1262-1271. https://doi.org/10.1021/acs.jmedchem.6b00990

Vivek-Ananth RP, Rana A, Rajan N, Biswal HS, Samal A. *In silico* identification of potential natural product inhibitors of human proteases key to SARS-CoV-2 infection. Scientific Reports 2020: 10(1), 12299. https://doi.org/10.1038/s41598-020-69274-5

Wang Z, Iris LK, Wong F, Yang C, Liu Z, Jiang T, Sheng B. Optimization of permethyl ningalin B analogs as P-glycoprotein inhibitors. Bioorganic & Medicinal Chemistry

2015: 23(17), 5566–5573. https://doi.org/10.1016/j.bmc.2015.07.027

Wankowicz SA, de Oliveira SH, Hogan DW, van den Bedem H, Fraser JS. Ligand binding remodels protein side-chain conformational heterogeneity. eLife 2022: 11, e74114. https://doi.org/10.7554/eLife.74114

Wendorff TJ, Schmidt BH, Heslop P, Austin CA, Berger JM. The structure of DNA-bound human topoisomerase II alpha: conformational mechanisms for coordinating inter-subunit interactions with DNA cleavage. Journal of Molecular Biology 2012: 424(3-4), 109-124. https://doi.org/10.1016/j.jmb.2012.07.014

Whitson EL, Bugni TS, Chockalingam PS, Concepcion GP, Harper MK, He M, Hooper JN, Mangalindan GC, Ritacco F, Ireland CM. Spheciosterol sulfates, PKCzeta inhibitors from a philippine sponge *Spheciospongia* sp. Journal of Natural Products 2008: 71(7), 1213–1217. https://doi.org/10.1021/np8001628

Yerien, DE, Bonesi S, Postigo A. Fluorination methods in drug discovery. Organic & Biomolecular Chemistry Journal 2016. https://doi.org/10.1039/C6OB00764C

Zhang QT, Liu ZD, Wang Z, Wang T, Wang N, Wang N, Zhang B, Zhao YF. Recent Advances in Small Peptides of Marine Origin in Cancer Therapy. Marine Drugs 2021: 19(2), 115. https://doi.org/10.3390/md19020115

Zheng LH, Wang YJ, Sheng J, Wang F, Zheng Y, Lin XK, Sun M. Antitumor peptides from marine organisms. Marine Drugs 2011: 9(10), 1840–1859. https://doi.org/10.3390/md9101840

SUPPLEMENTARY MATERIAL

Receptor (PDB ID)	Co-crystallized Ligand	Superimposition of Co-crystal (red) and its redocked structure (blue)	RMSD
4UND	(8S,9R)-5-fluoro-8-(4-fluorophenyl)-9-(1-methyl-1H-1,2,4-triazol-5-yl)-2,7,8,9-tetrahydro-3H-pyrido[4,3,2-de]phthalazin-3-one	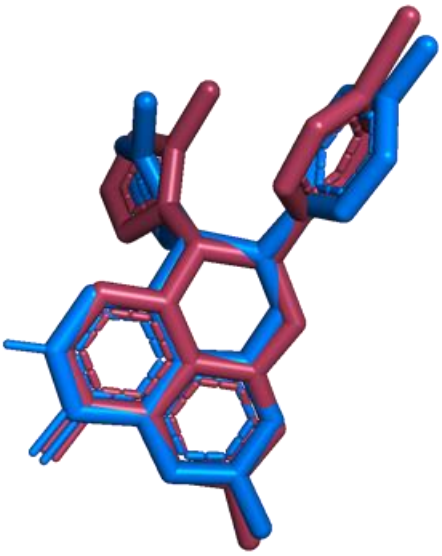	0.666 Å
3MAX	N-(4-aminobiphenyl-3-yl)benzamide	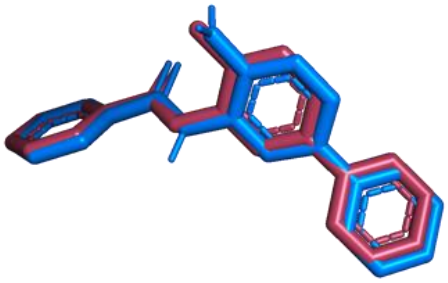	1.038 Å
1T8I	4-ethyl-4-hydroxy-1,12-dihydro-4h-2-oxa-6,12a-diaza-dibenzo[b,h]fluorene-3,13-dione	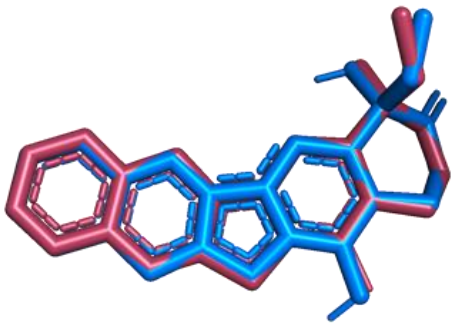	0.364 Å
4FM9		*No co-crystallized ligand*	